TECHNICAL REPORT BRL-TR-2888

BRL

1938 – Serving the Army for Fifty Years – 1988

THE TRANSITIONAL BALLISTICS, AEROBALLISTICS AND JUMP CHARACTERISTICS OF A 25-MM-AP TRAINING PROJECTILE WITH BASE BLEED

PETER PLOSTINS
JONATHAN A. BORNSTEIN
CHARLES O. WHITE

MARCH 1988

U.S. ARMY LABORATORY COMMAND

BALLISTIC RESEARCH LABORATORY

ABERDEEN PROVING GROUND, MARYLAND

DESTRUCTION NOTICE

Destroy this report when it is no longer needed. DO NOT return it to the originator.

Additional copies of this report may be obtained from the National Technical Information Service, U.S. Department of Commerce, Springfield, VA 22161.

The findings of this report are not to be construed as an official Department of the Army position, unless so designated by other authorized documents.

The use of trade names or manufacturers' names in this report does not constitute indorsement of any commercial product.

UNCLASSIFIED
SECURITY CLASSIFICATION OF THIS PAGE

REPORT DOCUMENTATION PAGE

Form Approved
OMB No. 0704-0188

1a. REPORT SECURITY CLASSIFICATION UNCLASSIFIED	1b. RESTRICTIVE MARKINGS
2a. SECURITY CLASSIFICATION AUTHORITY	3. DISTRIBUTION/AVAILABILITY OF REPORT
2b. DECLASSIFICATION/DOWNGRADING SCHEDULE	
4. PERFORMING ORGANIZATION REPORT NUMBER(S) BRL-TR-2888	5. MONITORING ORGANIZATION REPORT NUMBER(S)
6a. NAME OF PERFORMING ORGANIZATION U.S. Army Ballistic Research Laboratory 6b. OFFICE SYMBOL (If applicable) SLCBR-LF	7a. NAME OF MONITORING ORGANIZATION
6c. ADDRESS (City, State, and ZIP Code) Aberdeen Proving Ground, MD 21005-5066	7b. ADDRESS (City, State, and ZIP Code)
8a. NAME OF FUNDING/SPONSORING ORGANIZATION U.S. Army Ballistic Research Laboratory 8b. OFFICE SYMBOL (If applicable) SLCBR-DD-T	9. PROCUREMENT INSTRUMENT IDENTIFICATION NUMBER
8c. ADDRESS (City, State, and ZIP Code) Aberdeen Proving Ground, MD 21005-5066	10. SOURCE OF FUNDING NUMBERS PROGRAM ELEMENT NO.: RDT&E PROJECT NO.: 1L162618 TASK NO.: AH80 WORK UNIT ACCESSION NO.

11. TITLE (Include Security Classification)
The Transitional Ballistics, Aeroballistics and Jump Characteristics of a 25mm-AP Training Projectile with Base Bleed

12. PERSONAL AUTHOR(S)
Plostins, Peter, Bornstein, Jonathan A., White, Charles O.

13a. TYPE OF REPORT	13b. TIME COVERED	14. DATE OF REPORT (Year, Month, Day)	15. PAGE COUNT
Final	FROM _____ TO _____	1988 March	

16. SUPPLEMENTARY NOTATION

17. COSATI CODES			18. SUBJECT TERMS (Continue on reverse if necessary and identify by block number)
FIELD	GROUP	SUB-GROUP	
01	01		APFSD-T Ammunition, Training Ammunition, ~~Aeroballistics~~
19	01		APTP-T Ammunition, ~~Transitional~~ Ballistics, ~~Base Bleed~~
			APDS-T Ammunition, ~~Ammunition, Jump~~ SPIN-STABILIZED AMMUN

19. ABSTRACT (Continue on reverse if necessary and identify by block number)

A sabot launched spin-stabilized training projectile is being developed by the U.S. Army for the 25mm cannon. The training projectile is required to ballistically match the present service projectile. The ballistic match requirements are stringent and the transitional ballistics, aeroballistics and jump characteristics of the training projectile must be controlled to satisfy the requirements. This report presents the results of a series of tests which were designed to evaluate the transitional ballistics, aeroballistics and jump characteristics of the training projectile. The same tests are performed on the service projectile to provide a baseline for evaluation of the ballistic match. It was found that the training projectile did satisfy the maximum range requirement of 8000 meters. The jump characteristics of the training projectile and the service projectile are different enough to cause concern about the ability of the training projectile design to meet the center of impact requirement on the target.

20. DISTRIBUTION/AVAILABILITY OF ABSTRACT ☒ UNCLASSIFIED/UNLIMITED ☒ SAME AS RPT. ☐ DTIC USERS	21. ABSTRACT SECURITY CLASSIFICATION UNCLASSIFIED
22a. NAME OF RESPONSIBLE INDIVIDUAL Peter Plostins	22b. TELEPHONE (Include Area Code) 301-278-3786
	22c. OFFICE SYMBOL SLCBR-LF-E

DD Form 1473, JUN 86 — Previous editions are obsolete. — SECURITY CLASSIFICATION OF THIS PAGE

INTENTIONALLY LEFT BLANK.

TABLE OF CONTENTS

INTENTIONALLY LEFT BLANK.

LIST OF FIGURES

LIST OF FIGURES (CONTINUED)

LIST OF FIGURES (CONTINUED)

INTENTIONALLY LEFT BLANK.

I. INTRODUCTION

The U.S. Army is developing a training round for the 25mm cannon. This training projectile is to be used in lieu of the present service ammunition as well as future service ammunition. The current combat ammunition is a spin-stabilized, armor-piercing, discarding sabot, traced projectile, "APDS-T," see Figure 1a. It will soon be replaced with an armor-piercing, fin-stabilized, discarding sabot, traced projectile, "APFSDS-T," see Figure 1b. In the interim, it is desired that the training round ballistically match both the APDS-T and the APFSDS-T ammunition. The requirements for an aeroballistic match are summerized below.

(1) The time of flight difference between the APTP-T and the service projectiles will be less than 0.50 s at 2000 meters.

(2) The center of impact of the APTP-T will not vary from that of the service ammunition by more than 1 mil from 0 to 2000 meters.

(3) The APTP-T will have a maximum range of 8000 meters which includes the ricochet safety danger zone.

(4) The APTP-T will have a visible trace from 100 meters to at least 2000 meters.

(5) The APTP-T will have a dispersion that does not exceed the dispersion of the service ammunition by more than 10%.

A variety of possible training round candidates were evaluated to determine if they would meet the requirements. Configurations considered included: a) flare stabilized long rods,[1] b) vented flare "LKL" long rods,[2,3], c) tubular projectiles,[4,5] and d) spin-stabilized, de-spin and fin-stabilized projectiles.[6] Based on preliminary evaluation of the latter candidates, it was concluded that a spin-stabilized, armor-piercing, target practice, traced projectile, "APTP-T," should be developed. The APTP-T round would be sabot launched and similar in configuration to the present APDS-T service projectile, see Figure 2. To achieve the required ballistic match, the APTP-T would utilize a tracer as a base bleed mechanism to reduce the total drag early in the trajectory. After tracer burnout, the resulting high drag in combination with a low ballistic coefficient would limit maximum range.

Focus of the present report is on evaluation of the capability of the APTP-T concept to meet requirements (2) and (3). The other requirements are or can be satisfied. The time of flight requirement, (1), is easily met, as described in Reference 6. The trace requirement, (4), is met by using a design which combines the projectile trace/base bleed functions into a single mechanism. The projectile dispersion requirement, (5), is a complex design problem beyond the scope of the present report. However, a well designed and manufactured projectile/sabot combination will meet this requirement.

Requirement (2) states that the training projectile must remain within one milliradian of the service projectile for the first 2000 meters. This

poses a severe design challenge because jump characteristics can differ significantly, even for rather similar projectile design configurations. Jump is defined as the angular deviation of the projectile from the pre-shot line-of-fire by causes other than gravity drop. Factors governing projectile jump behavior include:

(1) The gun dynamics of the cannon. Axial, horizontal and vertical motion of the cannon, prior to shot exit, cause the muzzle to deviate from the pre-shot line-of-fire at shot exit.

(2) Projectile inbore balloting and muzzle disengagement disturbances are such that the projectile CG velocity vector is not coincident with the bore centerline at shot exit.

(3) Sabot discard perturbations that further alter the linear and angular motions of the projectile.

(4) Free flight initial conditions that result in aerodynamic jump, see Reference 7.

Differences in projectile weight, inertial properties, CG location, muzzle velocity and aerodynamic characteristics cause different responses to the above factors. This is why the jump of the spin-stabilized APTP-T training projectile will be different from that of the spin-stabilized APDS-T service projectile or the fin-stabilized APFSDS-T service projectile. Tests to evaluate these interactions are reported herein as Section II: "Transitional Ballistics and Jump Characteristics." These tests measure and compare the entire ballistic trajectories of the APTP-T and the APDS-T projectiles from muzzle exit to target impact, over a range of 100 meters. The testing was conducted in the U.S. Army Ballistic Research Laboratory Aerodynamics Range Facility, "ARF." From the test data, the sources of the projectile jump could be identified and quantified. The APFSDS-T projectile was not tested because the design has not yet been finalized. It will be tested in the near future.

Requirement (3) of the projectile specifications states that the projectile maximum range shall not exceed 8000 meters. The actual range of the projectile must be shorter to accommodate the ricochet fan. To evaluate the maximum range trajectory performance of the APTP-T projectile, the aerodynamic characteristics of the projectile must be known over a Mach number range from 0.5 to 4.5. Information required includes drag, pitching moment, lift, pitch damping moment and Magnus moment coefficients. Tests to evaluate these coefficients are reported herein as Section III; "Aeroballistic Characteristics." The basic aerodynamic characteristics of the projectile were measured in the ARF. Data on the traced projectile were obtained in the Transonic Range Facility, "TRF," of the U.S. Army Ballistic Research Laboratory. The TRF has 25 orthogonal spark shadowgraph stations and is a larger facility capable of recording the flight of artillery projectiles, see Reference 8. The TRF was used for the test because the film plane in the ARF is too close to the line-of-fire and traced ammunition over exposes the film destroying and image of the projectile. The aerodynamic coefficients obtained from these tests were used to predict the maximum range trajectory for comparison with Midi radar measurements performed at Ft. Bliss, Texas. Comparisons between the analytically predicted and experimentally measured maximum range trajectories are presented in Section III.

II. TRANSITIONAL BALLISTICS AND JUMP CHARACTERISTICS

1. TEST SETUP, INSTRUMENTATION, DATA ACQUISITION AND REDUCTION

The transitional ballistics and jump tests test were conducted in the Aerodynamics Range Facility which consists of a series of 30 orthogonal spark shadowgraph stations. A schematic of the setup is given in Figure 3. The range coordinate system has its origin 4.57 meters in front of the first shadowgraph station. The Z axis runs downrange, the Y axis is positive up and the X axis is positive to the right looking downrange. The Z axis lies along the lower right corner of the range stations. The muzzle of the cannon is located at Z=-.58 meter. This coordinate system is used to locate all of instrumentation used in the test.

To measure the effect of the gun dynamics on the jump, the position and angular orientation of the muzzle at shot exit must be recorded. The recoil of the gun is measured by a reflective optical scanner, manufactured by Skan-A-Matic Corporation. It consists of an LED light source surrounded by a detector. When reflected light is detected the probe emits a 5-volt pulse. A target of black and white strips, 0.254 cm in width, is placed on the barrel near the breech, see Figure 4. As the gun recoils, the target moves under the probe and generates a series of square pulses. Each pulse represents 0.254 cm of recoil travel. The recoil position at shot exit can be calculated from the number of pulses up to that time. In Figure 4, the Kistler piezoelectric gage used to monitor the case mouth pressure can also be seen. The case mouth pressure and optical scanner output are recorded on Nicolet Digital Oscilloscopes. Figure 5 shows a typical plot of the output from the case mouth pressure gage and the output of the optical scanner. Shot exit occurs at zero milliseconds and the cannon has only recoiled 0.25 centimeter. The propellant pressure starts to increase about 2.25 milliseconds prior to shot exit and the cannon begins to recoil after peak propellant gas pressure occurs. The data are for the APDS-T projectile fired at a muzzle velocity of 1325 m/s.

The horizontal and vertical position of the muzzle are recorded using model M61 radio frequency proximity sensors manufactured by Scientific Atlanta Incorporated. Four probes, spaced 90 degrees apart are placed around the outer circumference of the gun tube at two axial stations near the muzzle. In range coordinates, eddy probe Station (1) is located at Z=-0.89 meter and Station (2) at Z=-0.77 meter. Figure 6 shows the arrangement of the eddy probes. The output signal of the devices is proportional to the width of the gap between the probe and the gun. Data are initially stored on magnetic disks by Nicolet Digital Oscilloscopes and later transferred to a VAX 8600 computer for processing. The proper addition and subtraction of the voltage obtained from opposing probes permits the determination of the transverse gun tube motion as a function of time. Complete details of the data analysis procedure can be found in Reference 9. The linear range of the gages used is 0.5 to 2.0 millimeters. By determining the relative translation of the gun tube at the two closely spaced locations, it is possible to determine the muzzle pointing angle. Using the transverse linear velocity at Station (1), the angular velocity of the gun tube and the distance from Station (1) to the muzzle, the muzzle crossing velocity is calculated. Figures (7a-7b) are typical plots of the displacement of the cannon in the horizontal and vertical planes respectively. Figures 8a-8b are the corresponding muzzle pointing

angle in radians. The data are for the APDS-T projectile launched at a muzzle velocity of 1325 m/s. The spikes in the data just after shot exit are due to x-rays pulsing as the projectile moves downrange. The muzzle pointing angle and crossing velocity are the jump contributions due to the gun dynamics.

As the projectile leaves the muzzle, it enters the transitional ballistic phase. During this phase the projectile disengages from the muzzle, passes through the reverse flow of the propellant gases, penetrates through the muzzle blast wave and discards its sabot and base. The linear and angular motions during this phase are recorded by six orthogonal x-ray stations, see Figure 9. Each x-ray station consists of a pair of Hewlett Packard 150 KV x-rays. Soft x-ray tubes were used in the x-ray heads so that the plastic sabot would be captured on the x-ray image. The x-ray image is recorded on Kodak XM840 film. The film is loaded into two long x-ray cassettes that are fitted with Dupont Cronex intensifying screens. The cassettes are then placed on the horizontal and vertical film planes, using the plywood surfaces shown in Figure (9). The six x-ray stations are nominally located at Z = -0.53 m, -0.28 m, -0.08 m, +0.58 m, 1.27 m and 1.58 m. The x-ray stations are triggered in a delayed sequence to fire as the projectile arrives at each station. Hewlett Packard delay units are used to set the delays and Hewlett Packard digital counters record the time of the actual x-ray firing pulses.

The linear and angular motion recorded on the x-ray film must be tied into the ARF coordinate system. A fiducial cable is used to provide this reference on the x-ray images. Prior to firing, the fiducial cable is hung through the x-ray stations and the first group of range stations. The fiducial cable is centered in the muzzle, see Figure 10, and in a target located at a range station located at Z=12.0 meters , see Figure 11. A boresight is used to place the downrange target on the line-of-fire. Using this technique, the cable is placed along the line-of-fire. A low level x-ray of the cable is taken prior to the test, the cable is then removed and a second x-ray of the projectile is taken during the test; thus, a double image of the cable and the test projectile result. A simple data reduction technique may now be used to extract the linear and angular orientation of the projectile, as described in Reference 10. The magnitude of the errors using this technique are discussed in Reference 11. To locate the muzzle and tie the position of the x-ray stations into the range coordinate system, a series of beads are placed on the fiducial cable. A bead is located directly at the intersection of the x-ray heads and the line-of-fire and another 5.08 cm downrange, see Figure 9. The two beads at the x-ray heads provide range coordinate reference points and local image magnification. The actual distance between the beads is known and by measuring the distance between the beads on the x-ray image, the magnification ratio is computed. Also one bead is located at each of the first five ARF stations. These beads link the cable to the range coordinate system. The cable catenary and spatial orientation are calculated from this data. All x-ray and range instrumentation are now uniquely defined in a common coordinate system.

After the projectile discards its sabot and base, it enters free flight. Free flight occurs before the last x-ray station and the projectile is in free flight as it enters the ARF. The 30 orthogonal spark shadowgraph stations photograph the linear and angular motion of the projectile over a distance of 100 meters. The ARF is controlled by a Hewlett Packard HP1000 computer system that sets the delays for all the range stations. Reference 7

describes the data reduction techniques used to determine the free flight aerodynamic characteristics of the projectile. The drag, lift, static moment, Magnus moment and pitch damping moment coefficients are determined from the flight data. At the end of the range the projectile impacts on a 100-meter target.

To provide a reference for all the components of the jump, the pre-shot line-of-fire must be determined. A boresight is placed in the muzzle of the cannon and collimated. The boresight, manufactured by the Lenzar Optics Corporation, did not have external collimation adjustments. Therefore, the boresight was collimated on the target, see Figure 12. The boresight is rotated in 90 degree increments and the cross hair location is recorded on the target. The initial reading is at 90 degrees with subsequent readings at 180, 270 and finally zero degrees; see data points in Figure 12. A least-squares-fit technique is then applied to the circle of four points and the center of the circle is taken as the actual aimpoint of the borescope. The nominal error in locating the center of the circle is 0.075 mil. The spatial orientation of the line-of-fire in the range coordinate system must now be obtained. The borescope is not moved and is left at the zero degree position. A series of spheres are then placed on the line-of-fire by sighting them into position using the borescope, see Figure 13. Five spheres are used, nominally located at Z= 4.5, 7.6, 9.2, 10.7 and 12.2 meters. These positions correspond to range stations and the sphere locations are recorded on film. A straight-line fit through the coordinates of the muzzle and the five spheres (corrected to the borescope aimpoint) provides the static line-of-fire.

The preceding paragraphs have described how the instrumentation is tied together in the range coordinate system. A common-time base is also needed. A piezoelectric gage is located at the muzzle of the cannon, see Figure 6. When the gun is fired, the gage senses the pressure due to the propellant blast wave; thus, the blast wave pressure pulse triggers all the instrumentation. Again, Nicolet Digital Oscilloscopes are used to record the signal. The pressure gage is a finite distance from the muzzle and it takes the blast wave a small amount of time to arrive at the gage; therefore, the projectile travels downrange and the gun recoils before the wave is sensed by the gage. Trigger time zero is corrected to account for this delay.

Twelve rounds were made available to perform the jump tests, six each APDS-T and APTP-T projectiles. Of the six APDS-T projectiles, four were used to calibrate the triggering system. One of the APDS-T projectiles was launched at a very low yaw level and the quality of the aeroballistic results from the ARF and the x-rays is in questionable. This is because the root mean square error in the data fit is as large as the measured data. One good APDS-T data round was successfully launched. Two of the APTP-T rounds failed to trigger the stations in the ARF. Good data were obtained on the other four APTP-T projectiles. Two of the four were launched with different charges to obtain drag data without a tracer. The final two were launched at approximately the design velocity for a ballistic match to the APDS-T.

2. ANALYSIS OF THE DATA

As previously stated, the gun dynamics contribute to the jump of the projectile off the pre-shot line-of-fire. The gun tube is mounted in a recoil system, (in this case a laboratory recoil system), and the center of mass of

the recoiling parts is not necessarily on the recoil axis. The gun is forced to recoil by the breech pressure exerted by the propellant gases. This force is generally on the recoil axis; therefore, the gun exhibits translation and rigid body motion within the constraints of its mounting. The gun tube is also a long flexible member that bends in response to the forcing functions provided by the pressure on the breech and the projectile interacting with the bore as the projectile is accelerated. The combination of these forces causes the muzzle to have a different linear and angular position, as well as a velocity at the instant of shot exit. The important contributions to jump come from the angular position of the gun and the transverse velocity of the muzzle that is imposed on the exiting projectile. Figure 7a gives the displacement of the barrel at Stations (1) and (2) respectively. Station (2) is located closest to the muzzle. At shot exit the displacement at Station (1) is further to the left than at Station (2); therefore, the gun is pointing to the right as indicated in Figure 8a. Figure 7b describes the motion of the gun in the vertical plane. The gun displacement at Station (1) is higher than at Station (2) so the gun points down at shot exit, Figure 8b.

The data described above are for the APDS-T projectile but is indicative of the data for all the rounds fired, see Figures 14a, 14b and 14c. The data in Figure (14a) compares the vertical muzzle pointing angle for four different rounds at different conditions. Qualitatively, the dynamic motion of the cannon appears to be the same. The difference in amplitude of the negative peak near shot exit can be related to the impulse delivered to the cannon prior to shot exit. Equation (1) provides an estimate for the impulse given to the cannon prior to shot exit.

$$I = MV \left(1 + \frac{1}{2}\frac{C}{M}\right) \qquad (1)$$

In the equation, M is the mass of the projectile, C is the propellant mass and V is the muzzle velocity. The APDS-T projectile delivers an impulse of 244 kg-m/s. The two APTP-T projectiles fired at 1500 m/s have the second highest impulse: 216 kg-m/s; and the slow APTP-T projectile the lowest; 203 kg-m/s. It is believed that the dominant forcing function causing cannon motion in the vertical plane is the breech pressure which when integrated in time is the impulse as defined by Equation (1). The center of mass of the recoiling parts is below the boreline of the cannon, thus, allowing for rigid body rotation of the cannon about the mass center within the constraints of the mounting. The cannon used is a stiff Mann barrel, so very little of the angular motion of the gun in the vertical plane is due to dynamic tube bending. Figure (14b) is an expanded view of the motion near shot exit. Shot exit is marked by the x on each curve. Each round exits at a different cannon pointing angle and cannon angular velocity. The vertical gun dynamics of the two fastest APTP-T projectiles appears very similar.

The correlation with impulse found for the angular motion in the vertical plane does not appear to hold for the motion in the horizontal plane, see Figure 14c. Again, the angular motion of the cannon is similar for the different projectiles fired. All of the forces driving the gun motion in the horizontal lie in the symmetry plane of the recoiling parts. One dominant force cannot be identified, so it appears that the gun motion is a sum of the pressure force on the breech and the projectile/bore interaction forces. One

final note on the horizontal motion; the initial slope of the motion is non-zero. This cannon is fired by pulling a lanyard and the offset in initial angle and angular rate is a response to the lanyard force. The cannon is not as constrained by the recoil system in the horizontal as it is in the vertical plane, so it is free to move in response to the lanyard force. To determine whether the lanyard pull had clouded any correlation in the data, the effects of the lanyard pull were removed, see Figure 15. The angle and angular rate of the cannon just prior to shot start was extracted from the data; but, as before, the data in Figure 15 indicate the same trends as that in Figure 14a and no correlation to the impulse delivered to the breech is obvious.

The previous paragraphs have described how the gun motion causes the projectile to jump off the static pre-shot line-of-fire. The jump due to the gun motion is a sum of the dynamic gun pointing angle and the angle caused by the muzzle crossing velocity. This angle is simply the arc tangent of the linear muzzle crossing velocity divided by the projectile muzzle velocity. The inbore motion of the projectile relative to the cannon further contributes to the jump. The interactions between the projectile and the cannon bore during acceleration cause the projectile to have linear and angular rates at the muzzle that are different from those due to the gun motion alone. The disengagement of the projectile from the muzzle also alters the motion, as does the reverse flow of the high pressure propellant gas passing over the projectile base within the muzzle blast. Finally, asymmetrically discarding sabot components could further disturb the trajectory of the projectile.

Orthogonal x-rays are used to record the linear and angular rates of the projectile at muzzle exit as well as the disturbances due to the discarding sabot. Figures 16a-f are horizontal views of the APTP-T projectile, V=1432 m/s, at the six x-ray stations. At Station (1) the muzzle and the projectile are visible and the plastic sabot is just beginning to separate. The projectile has no discernible horizontal yaw. The plastic sabot is completely separated by Station (2) but the aluminum base is still engaged. By Station (3) the base is starting to separate and the projectile is beginning to yaw. The projectile is yawing and completely separated from its launch package at Station (4). At this point the projectile is entering free flight and the transitional ballistic disturbances are over. At Stations (5) and (6) free flight aerodynamic forces continue to increase the projectile yaw. The transitional ballistics of all the projectiles is qualitatively similar; the sabot discard is over approximately 0.5 to 0.6 meter downrange of the muzzle.

A quantitative analysis of the transitional ballistics is obtained by examining the motion of the projectile extracted from the x-ray images. Figures 17a and 17b are plots of the center of gravity, "CG," motion of the APTP-T projectile fired at V=1500 m/s. The projectile CG leaves the muzzle moving to the left and up from the pre-shot static line-of-fire. There are no distinctive changes in the linear CG motion in either plane, thus suggesting that this type of round experiences very little, if any, sabot discard disturbances. This is also reflected in the angular motion of the projectile during the transitional ballistic phase, see Figures 18a-d. The first figure observed gives the total yaw as well as the total yaw behavior calculated based on the measured angular rate at the muzzle. For reference, the fit of the free flight total yaw data measured in the ARF is also included. It is labeled "AR EXTRAPOLATION." The free flight aerodynamic behavior of the projectile measured in the ARF is reduced to aerodynamic coefficients

describing the free flight characteristics of the projectile. These aerodynamic coefficients were used to compute the total yaw curve labeled "MUZZLE PREDICTION." It is obvious that the total yaw based on the muzzle angular rates and that in free flight are almost the same. This leads to the conclusion that the sabot discard does not significantly disturb the flight of this projectile. This is in contrast to sabot discard disturbances observed for long-rod-kinetic-energy penetrators, Reference 12, where a distinct change in the angular rate of the projectile is evident subsequent to the mechanical disengagement of the sabot. Figures 18b, 18c, and 18d are plots of the components of yaw measured and the two predictions. No transitional ballistic disturbances are seen in either yaw plane. All of the other projectiles which were fired exhibit similar transitional ballistic characteristics. The net transitional ballistic effect on the jump for this class of projectiles is the jump of the CG trajectory off the dynamic line-of-fire defined by the gun dynamics. This contribution to the jump appears to be caused by inbore disturbances, disengagement disturbances, muzzle blast loads and maybe some minor sabot separation disturbances.

The ARF was used to measure the linear and angular behavior of the projectile in free flight during the 100 meter flight to the target. From the free flight measurements, the final contribution to the jump was obtained. The aerodynamic jump is the deviation of the mean CG trajectory from the initial CG velocity vector due to aerodynamic forces alone. The asymptotic theory of Reference 7 gives an equation for the aerodynamic jump in terms of the physical and aerodynamic characteristics of the projectile. This equation is only valid as downrange distance, in projectile calibers, approaches infinity. The target distance is too short to compute the aerodynamic jump from the asymptotic theory. The value of the aerodynamic jump in the range is still tainted by the swerve of the projectile. The initial direction of the velocity vector of the CG is determined from the x-ray data, so the aerodynamic jump could be extracted from the CG trajectory in the ARF. Figures 19a and 19b are the horizontal and vertical CG motion measured in the range for the APTP-T projectile fired at V=1500 m/s. The solid line is the nonlinear least squares fit of the data used to determine the lift coefficient. The effects of gravity are removed from the vertical trajectory and the data corrected for the absolute angle of the initial CG velocity vector and divided by the downrange distance to yield the aerodynamic jump in the range, see Figures 20 and 21. The aerodynamic jump has almost settled down to the asymptotic value. The actual jump of the projectile impact was recorded on the 100 meter target. The gravity drop of the projectile can easily be computed from the time-of-flight measured in the ARF.

3. DISCUSSION OF THE RESULTS

The jump data can be summarized by plotting the vector components of the jump measured by the various techniques and comparing them to the impact of the projectile on the target. Consider Figure 22; the vector diagram of the jump of the APDS-T projectile. The origin of the coordinates is the image of the pre-shot static line-of-fire on the target. The solid circle is the projectile impact point. The first component of the jump vector is the muzzle pointing angle; the second is angular deviation due to the muzzle crossing velocity; the third is the jump due to inbore disturbances, disengagement disturbances, muzzle blast disturbances and sabot discard disturbances; the fourth is the aerodynamic jump; and the final vector is the gravity drop. The projectile has jumped approximately 0.5 mil down and 0.35 mil to the right of

its intended aimpoint due to causes other than gravity. This is a net radial jump of approximately 0.6 mil that will remain with the projectile throughout its entire flight.

The jump of the two APTP-T projectiles launched at V=1500 m/s is given in Figure 23. It is interesting to note that both projectiles arrived at the target by almost the identical trajectory. The gun was pointing down and to the right, the muzzle crossing velocity is up and to the left, the CG jump off the muzzle is up and to the left and the aerodynamic jump is up and to the right. The aerodynamic jump nearly compensates for the other horizontal jump components and the gravity drop making the net jump small for this projectile. These are only a sample of two firings, but it indicates that a projectile fired from the same gun tube at the same conditions has repeatable launch disturbance. The inbore disturbances to the projectile must be sufficiently similar that the CG trajectory off the muzzle is nearly identical. The angular initial conditions are also almost identical; which is demonstrated by the similarity in aerodynamic jump. Further tests on a better statistical sample are needed to confirm this behavior. The jumps of the APDS-T projectile and the APTP-T projectiles are different. The net jump of the APDS-T projectile takes the projectile down and to the right on the target and the APTP-T projectiles jump slightly up and to the right. There is a one-milliradian difference in the fall of shot. The center of impact ballistic match requirement is not satisfied at 100 meters. The majority of the separation is in the vertical plane. The gravity drop at 1000 meters of the APTP-T is 2.665 milliradians and of the APDS-T is 2.965 milliradians. The on target separation of the projectiles will, therefore, only increase at 1000 meters.

To satisfy Requirement (2), it is necessary to minimize the projectile jump. The jump due to gun dynamics is greater for the APDS-T projectile than it is for the APTP-T projectiles. These projectiles were fired from a Mann barrel in a laboratory recoil system and it cannot be assumed that the trend will remain the same in the service cannon. Tests should be performed to determine the gun dynamics of the service cannon. The linear and angular rates with which the projectile leaves the muzzle determine the level of the CG jump and the aerodynamic jump. Every attempt should be made to minimize these rates. These rates are controlled by the inbore disturbances. The bore straightness of the cannon probably plays a role as well as the flexural stiffness of the projectile sabot in determining the level of inbore disturbances imparted to the projectile. Reference [12] found that the angular rate of sabot-launched-long-rod projectiles could be minimized by stiffening the front sabot borerider. The front sabot borerider of both the APTP-T and APDS-T projectiles is plastic and, therefore, quite flexible. Changes in the design and stiffness of the borerider will influence the dynamic state of the projectile at the muzzle and may reduce the launch rates.

III. AEROBALLISTIC CHARACTERISTICS

1. DESCRIPTION OF THE TESTS

The jump characteristics of the APTP-T projectile were not known a priori, so it was designed to match the point mass trajectory of the APDS-T projectile to the target range of 2000 meters and remain within the 1

milliradian limits. Comparing the projectile characteristics of the APDS-T, Figure 1, and the APTP-T, Figure 2, it is evident that the APTP-T has a lower ballistic coefficient, is larger in diameter, has a conical nose rather than an ogival nose and is launched at a higher muzzle velocity. The higher muzzle velocity is not adequate to achieve a ballistic match to the APDS-T projectile. The tracer in the APDS-T projectile is only there to make it visible to the gunner. The tracer in the APTP-T serves two purposes; first, to provide visible light and second, to reduce the base drag of the projectile sufficiently, so that a point mass trajectory match is possible out to 2000 meters. The primary objective of the aeroballistic tests was to assess the base drag reduction capabilities of the tracer. This would define the ballistic match trajectory out to 2000 meters and provide a drag versus Mach number history to predict the projectile maximum range.

Three independent tests were performed, two of the tests were performed at BRL and a radar tracking test was conducted at Ft. Bliss, Texas. One test, at the ARF, measured the untraced drag and the other aerodynamic characteristics of the projectile; and the second, at the TRF, measured the traced drag of the projectile. Aeroballistic measurements on the untraced aeroballistic characteristics of the projectile were also available from the transitional ballistic test. The final test was conducted at the Ft. Bliss range facility. The projectiles were tracked with a point-position Midi radar. The data from this series of firings provided a complete drag verses Mach number history for the projectile as well as actual maximum range data.

The aeroballistic test of the untraced APTP-T was performed on a monolithic steel version of the APTP-T, Figure 24, designed by engineers at the Close Combat Armament Center, Combat Vehicle Ammunition Team, Picatinny Arsenal, Dover, New Jersey. It is similar to the projectile, Figure (2), used for all the other tests, which was designed by Ford Aerospace and Communications Corporation, Newport Beach, California.

The ARF and the TRF are described in the previous sections of the report. The data reduction techniques for obtaining aeroballistic information from these facilities are discussed in Reference 7. An example of the data acquired in the ARF is given in Figures 19a, 19b, 25a and 25b. The data are for the APTP-T projectile, untraced, launched at a muzzle velocity of 1500 m/s. Figures 19a and 19b are the measured CG motion of the projectile and the fit of the data in the horizontal and vertical planes, respectively. The total yaw and the yaw components with the corresponding data fits are given in Figures 25a and 25b.

2. ANALYSIS OF THE DATA

Range measurements were concentrated at supersonic Mach numbers between 3.5 and 4.5 because this is the expected flight regime out to 2000 meters. Some data were acquired at moderate supersonic Mach numbers around Mach 2.0; and the rest were taken at transonic Mach numbers. A limited number of projectiles were available for these tests; therefore, the data from the range firings is sparse at Mach numbers below 3.5.

The drag results from all of the tests are summarized in Figure 26. The drag coefficient of the untraced projectiles agrees well with the drag prediction of Reference 13, except at Mach 1.15. The drag coefficient of the

traced projectiles measured by the radar tests and the range tests also compare favorably. In the transonic regime, the prediction from Reference 13 is close to the drag measured by the radar. The drag data measured in the ranges have been corrected to reflect the drag at zero yaw. This is of course not true of the radar drag data. The dashed line in Figure 26 is the predicted drag of the projectile if the base drag were zero. Using this prediction as a reference, the tracer base bleed effect reduces the base drag of this projectile by approximately 60 to 70 percent at Mach 4.0. This is a reduction in total drag of 25 percent. Using the drag data, point mass trajectory predictions of the trajectory to the target were made, see Figure 27. For reference, the trajectory of the APDS-T projectile is included in the figure; as are the 1 milliradian bounds required by the ballistic match criteria. The maximum mismatch in the trajectories is only 0.30 milliradians at 1000 meters. As was pointed out in the previous section of the report this is the difference due to gravity effects without accounting for the effects of projectile jump.

The radar data obtained at Ft. Bliss, Texas provided maximum range data on the projectile. However, the data indicated that the maximum range was significantly less than expected. Ft. Bliss is located 1250 meters above sea level and the firings took place on a day when the ambient temperature was 32.2 degrees centigrade. The projectiles were temperature conditioned to 63 degrees centigrade, which resulted in a muzzle velocity of 1590 m/s. The data presented here are for a gun quadrant elevation of 32.5 degrees. The trajectory measured by the radar, Figure 28a, is very different from the point mass trajectory prediction. The point-mass-trajectory prediction used a drag versus Mach number history based on McDrag[13] and the known ARF and TRF drag data, see Figure 28b. Clearly the maximum range measured by the radar is significantly shorter than that of the prediction. The key to this anomaly can be found in the other aeroballistic characteristics of the projectiles. Figures 29a-d present the Mach number variations of the static moment, lift, pitch damping moment and Magnus moment. The data have not been corrected for the effects of yaw and the solid lines are faired curves that show the expected Mach number variation where no data are available. The faired curves are labeled "EST. CHARACTERISTICS." The key feature in Figure 29c is the change in the sign of the pitch damping moment between supersonic flight and subsonic flight. This change is characteristic of cone cylinder projectiles, Reference 7, and causes dynamic instability at subsonic Mach numbers. The Magnus moment also may cause stability problems in the subsonic regime, since it changes from a value near zero to a negative value.

A significant portion of the projectile flight is at subsonic Mach numbers and as the radar data indicate, the trajectory is affected by the flight dynamics. A six-degree-of-freedom, 6DOF, analysis of the trajectory was performed. The aerodynamic model for the 6DOF used the drag coefficient variation measured by the Midi radar with a constant subsonic drag coefficient of 0.24, together with the static moment, lift, pitch damping moment and Magnus moment variations presented in Figure 29 and a computed roll damping coefficient, see Figure 30. The roll damping coefficient was computed by the methods of Reference 13. A good first approximation for the yaw drag coefficient is the lift coefficient. Therefore, the model also used the lift coefficient variation in Figure 29b as input for the yaw drag coefficient. The 6DOF results presented are for the test conditions at FT. Bliss, see Figures 31a-e. The 6DOF prediction of height versus range is closer to the

actual radar data, see Figure 31a. The data indicate that the projectile flew at a lower velocity than that predicted by the 6DOF model along most of the trajectory, see Figure 31b. The initial yaw of the projectile for which the radar data were acquired is not known. The initial yaw used in the 6DOF model was 3.5 degrees and if the initial yaw of the projectile was higher during the radar test the velocity along the trajectory could shift as shown in the plot. From Figure 31c, a plot of dynamic stability factor versus range shows that the projectile loses its stability at 4000 meters. This range corresponds to a flight Mach number equal to one. The projectile remains unstable for almost 2000 meters, restabilizes, finally completely loses all stability and tumbles. During the period of dynamic instability the yaw grows, Figure 31d, and the projectile decelerates rapidly resulting in a radical increase in gyroscopic stability, see Figure 31e. The increase in gyroscopic stability causes the projectile to become dynamically stable for a short period just before it begins to de-stabilize for the final time. Both the radar data and the 6DOF analysis predict the round begins to tumble just after the peak in the trajectory. At that altitude it is impossible for the radar to lose track of the projectile. Rapid changes in the projectile deceleration along the trajectory were observed. The rapid changes in the deceleration are attributed to the rapidly changing radar cross section of the tumbling round. The radar data indicate that the projectile tumbles earlier than predicted by the 6DOF analysis, see Figure 32. Figure 32 is a plot of total drag at subsonic Mach numbers. Uncontrolled oscillations in the drag, measured by the radar, occur at Mach 0.4 whereas these oscillations are first predicted to occur at Mach 0.18 by the 6DOF analysis. Low level oscillations in the drag are already observed at Mach 0.9 in the data and no such behavior is computed by the 6DOF model. The linear aerodynamic model used in the 6DOF calculations is not adequate to accurately describe the motion of the projectile at subsonic Mach numbers. The 6DOF results, do however, qualitatively describe the nature of the mechanism that reduces the maximum range of this projectile.

Since the radar could not track the round accurately all the way to the ground plane and the 6DOF analysis was also unable to compute the trajectory to the ground plane, an alternate method of estimating the final leg of the trajectory was needed. Reference 14 presents drag data at subsonic Mach numbers for tumbling projectiles of various shapes. A drag coefficient of 2.93 was estimated for the APTP-T projectile. A point mass trajectory prediction for the tumbling APTP-T projectile was extrapolated to the ground plane for both the radar data and the 6DOF analysis, see Figure 33. The ground plane at Ft. Bliss is at 1250 meters altitude and both the extrapolation of the data and the 6DOF trajectories by this technique indicate the projectile impacts at approximately 7000 meters. This range is well below the maximum range limit of 8000 meters.

3. DISCUSSION OF THE RESULTS

The radar data show that all the projectiles fired at Ft. Bliss destabilize and begin to tumble within a Mach number range of 0.55 to 0.35. The 6DOF prediction gives a good qualitative understanding of the de-stabilization phenomenon but does not accurately predict the trajectory peak or the exact de-stabilization point, see Figures 32 and 33. The maximum range extrapolated from the data and the 6DOF results compare favorably. Further tests are needed to determine the precise linear and non-linear behavior of this

projectile at subsonic Mach numbers. Data should also be acquired at supersonic Mach numbers between 1.5 and 3.5. The 6 DOF trajectories are difficult to set up and time consuming to run; therefore, an interim prediction technique for the maximum range is required. A point mass trajectory based on the drag versus Mach number history in Figure 34 will predict the range to within five percent, see Figure 35. Between Mach 0.55 and 0.35 the drag coefficient is increased linearly to the tumbling round drag coefficient of 2.93. The high altitude at Ft. Bliss, the hot ambient temperature and the hot round muzzle velocity of 1590 m/s are an extreme case and will result in a long maximum range. The aerodynamic characteristics of this projectile insure that it can never exceed the maximum range limit specified. Most of the training will, however, occur at sea level; so for informational purposes three sea level trajectories are predicted using the interim point mass technique and are presented in Figure 36. The first trajectory is at standard sea level conditions and the muzzle velocity required for a ballistic match of 1500 m/s. The second is for standard sea level conditions and a hot projectile fired at V=1590 m/s. The final trajectory is the extreme case of a hot day and a hot projectile. The maximum sea level range for this projectile is 5890 meters.

IV. SUMMARY

A complete analysis of the factors affecting the ballistic match of the APTP-T training projectile to the APDS-T service projectile has been presented. Point mass calculations indicate that the APTP-T projectile will deviate a maximum of 0.30 milliradian from the trajectory of the APDS-T projectile due to gravity forces. The center of impact specification requires that the center of impact of the projectiles differ by no more than 1.0 milliradian. This means that there is a 0.70 milliradian margin for projectile jump effects. The impact difference due to projectile jump measured by the present tests is on the order of 1.0 milliradian. Obviously, the center of impact criteria is not met by the present APTP-T projectile. The projectiles tested were prototype configurations and it may be possible to reduce the jump effect.

The results of the jump tests should be considered in the proper context. The projectiles were launched from a Mann barrel and a laboratory recoil system, therefore, the gun dynamics contribution to the jump measured is not necessarily indicative of the gun dynamics effects of the service cannon. Tests are being set up to measure the gun dynamics of the service cannon. The linear and angular motion of the projectile subsequent to muzzle exit appears to be controlled by the linear and angular rates at the muzzle. Very few, if any, disturbances due to the mechanical disengagement of the sabot and pusher were observed. The dynamic state of the projectile at the muzzle is controlled by the inbore interaction dynamics of the flexible gun tube and the flexible sabot/projectile. Control of the tube straightness and the dynamic response of the flexible sabot may help reduce the linear and angular rates at the muzzle. One suggestion based on data in Reference [12] is to increase or vary the stiffness of the front sabot borerider. Based on the present results, it is imperative that the muzzle rates be reduced to insure a ballistic match.

The linear aerodynamic characteristics of the projectile were presented. It was found that the tracer-base-bleed mechanism reduced the total drag of the projectile by 25%. The measured aerodynamic coefficients and radar data along with 6DOF predictions indicate that the projectile is dynamically unstable at subsonic Mach numbers and, therefore, has a very short maximum range of 5890 meters at sea level. The instability results in very high drag coefficients below Mach 0.45. A drag versus Mach number history is presented which allows for point mass predictions of the maximum range to within 5%. This point mass prediction technique represents an interim solution until more extensive tests can be conducted to determine the exact linear and non-linear behavior of the projectile at subsonic Mach numbers. The results of the aeroballistic tests confirm that the projectile will not exceed the required maximum range of 8000 meters under any expected training conditions.

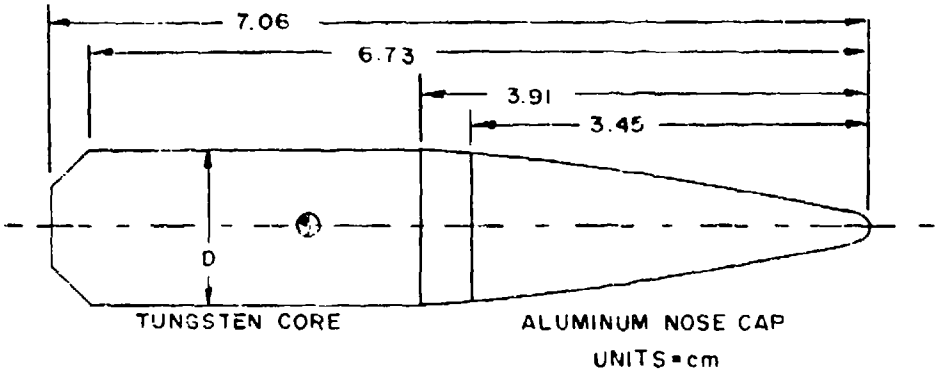

D = 1.35 cm
L/D = 5.24
M = 1045 gm
I_x = 21.9 gm-cm²
I_y = 176.0 gm-cm²
V = 1345 m/s
X_{cg} = 4.70 cm (from the nose)

Figure 1a. APDS-T projectile schematic.

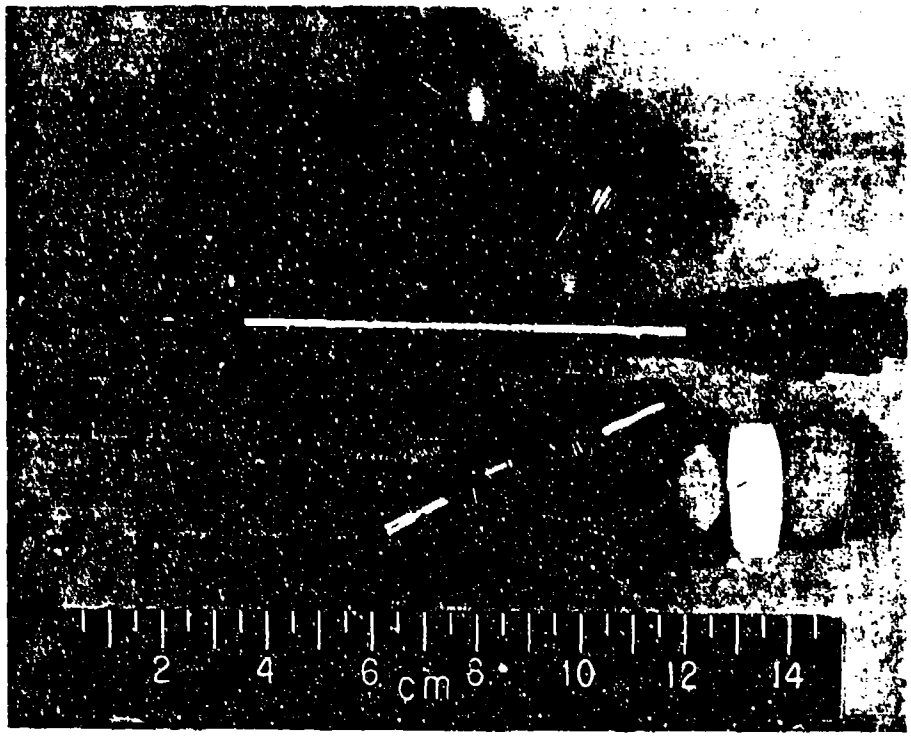

Figure 1b. APFSDS-T projectile photograph.

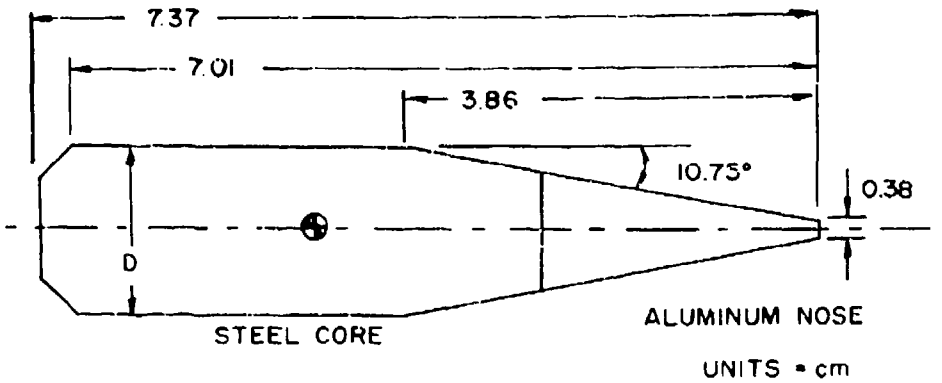

D = 1.65 cm
L/D = 4.47
M = 69.9 gm
I_x = 22.7 gm-cm²
I_y = 143.0 gm-cm²
V = 1500 m/s
X_{cg} = 4.75 cm (from the nose)

Figure 2. APTP-T projectile schematic.

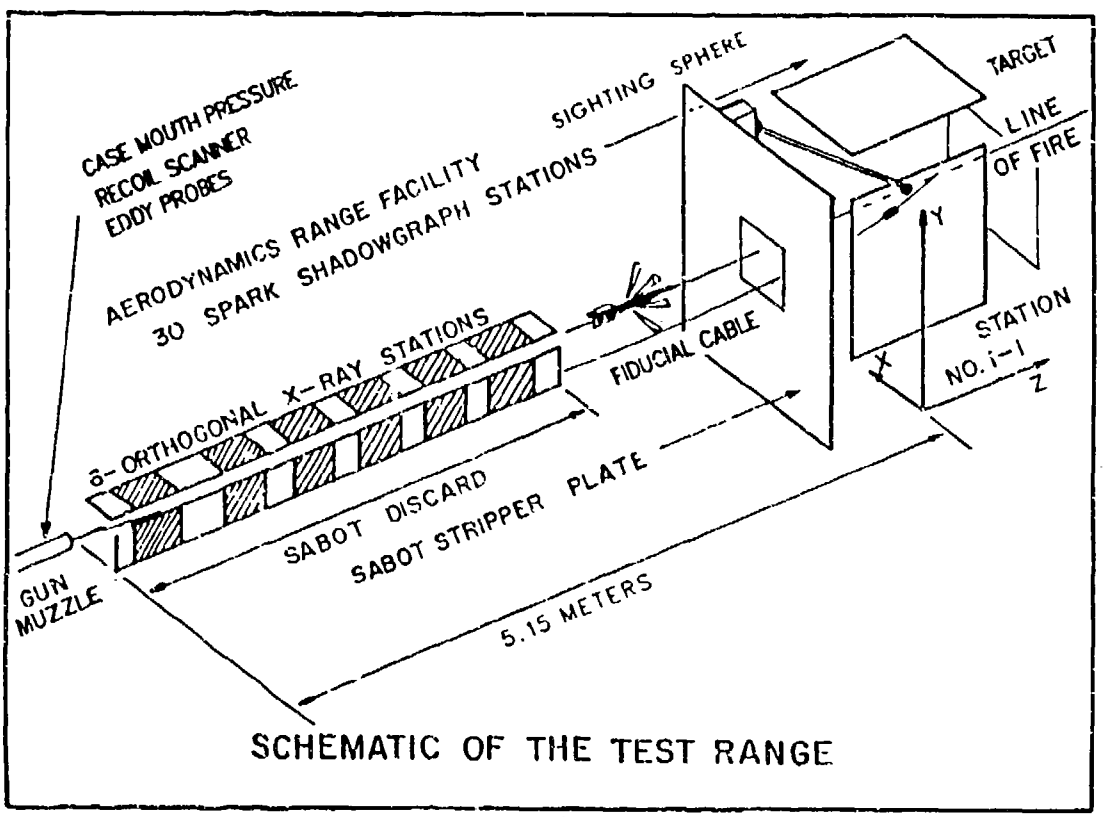

Figure 3. Schematic of the jump test setup.

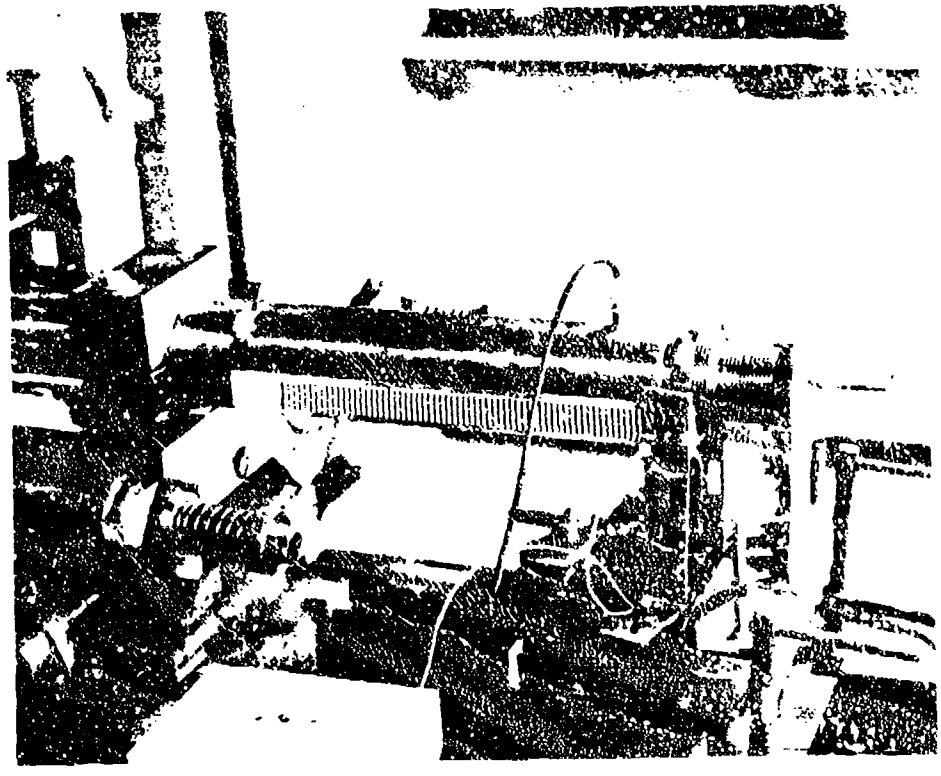

Figure 4. Optical scanner and case mouth pressure gage.

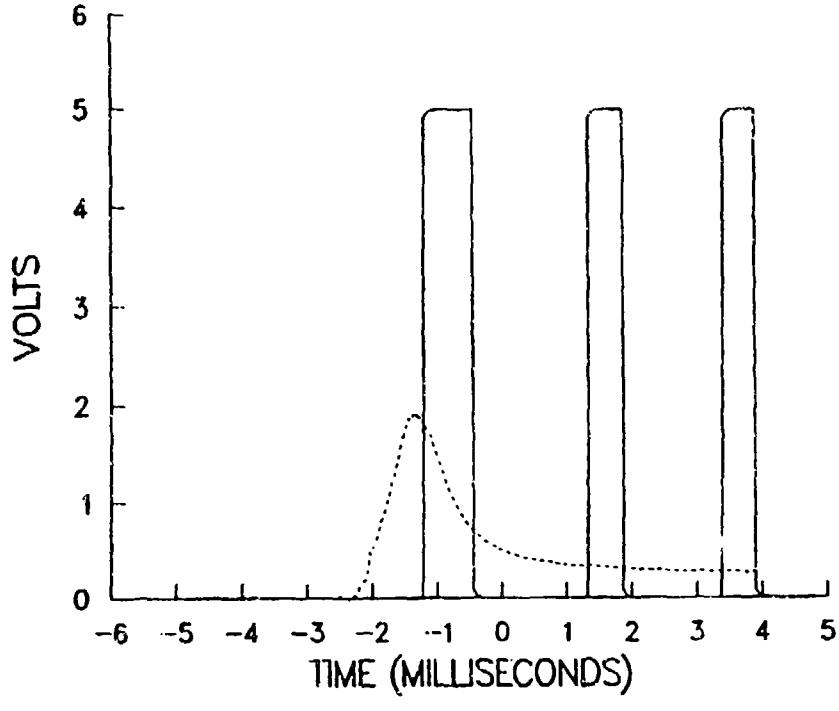

Figure 5. Optical scanner and case mouth pressure gage output.

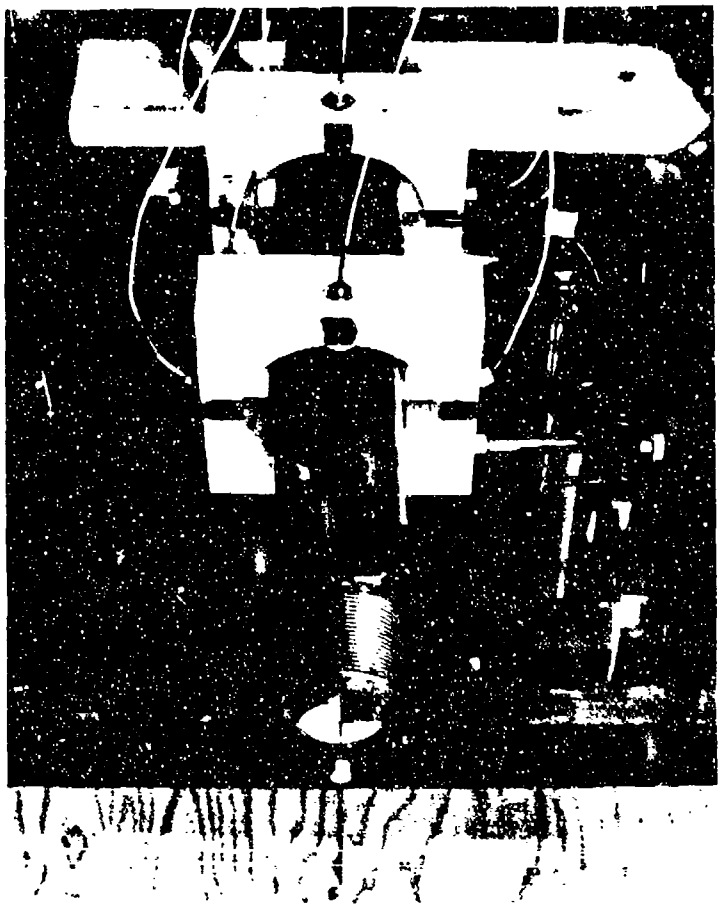

Figure 6. Proximity gage array at the muzzle.

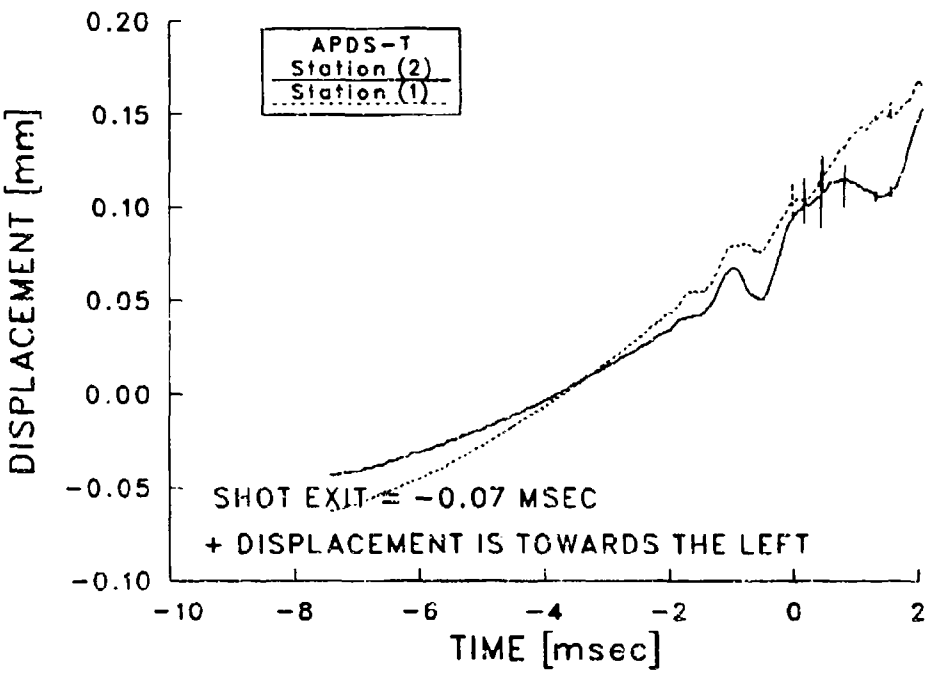

Figure 7a. Horizontal gun displacement: APDS-T projectile.

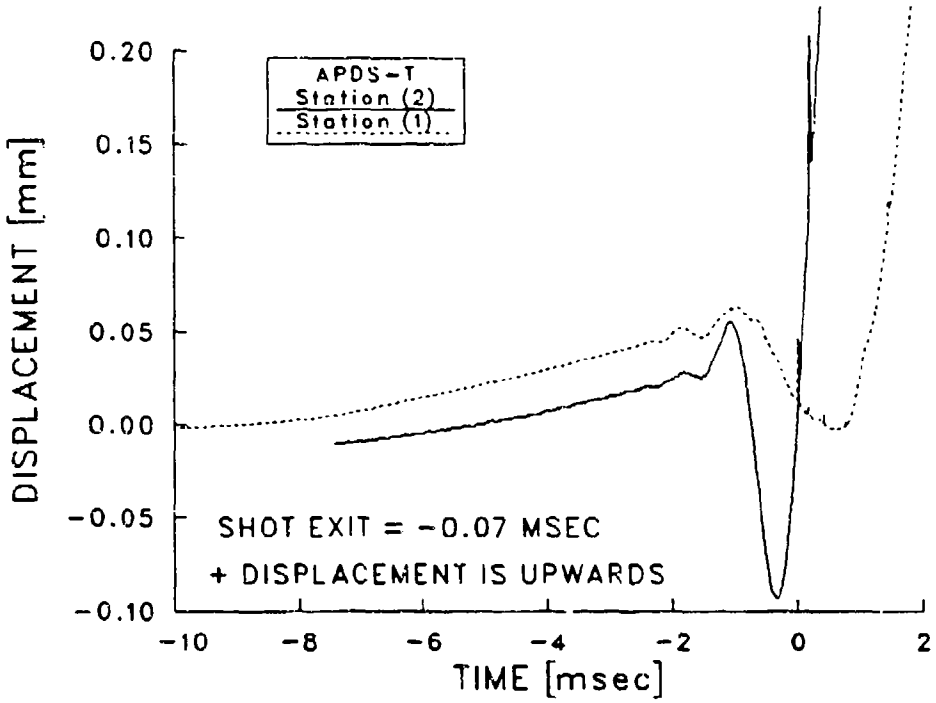

Figure 7b. Vertical gun displacement: APDS-T projectile.

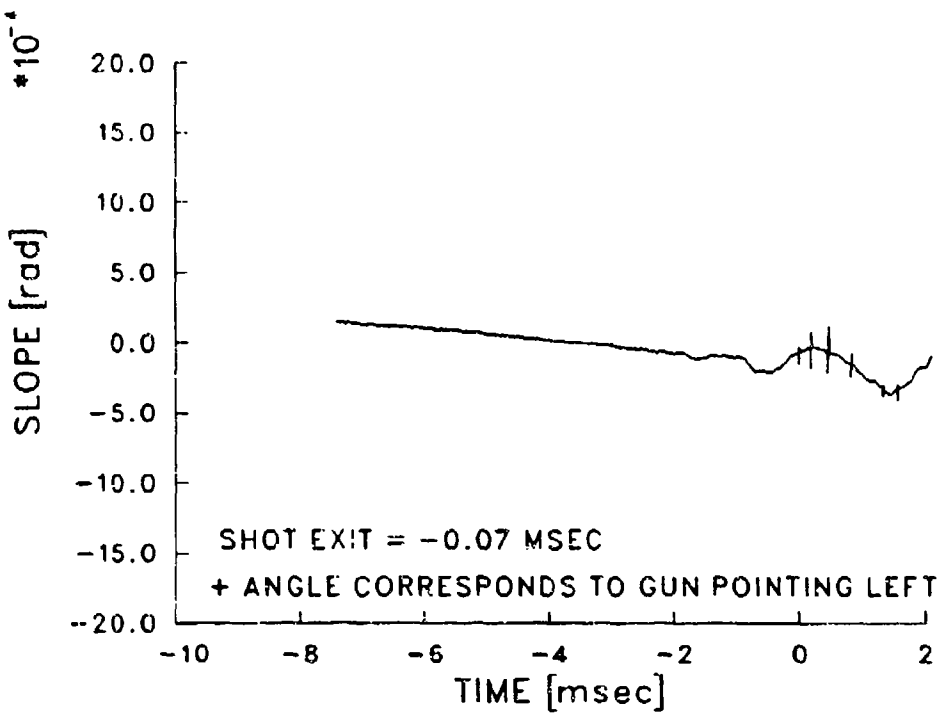

Figure 8a. Horizontal muzzle pointing angle: APDS-T projectile.

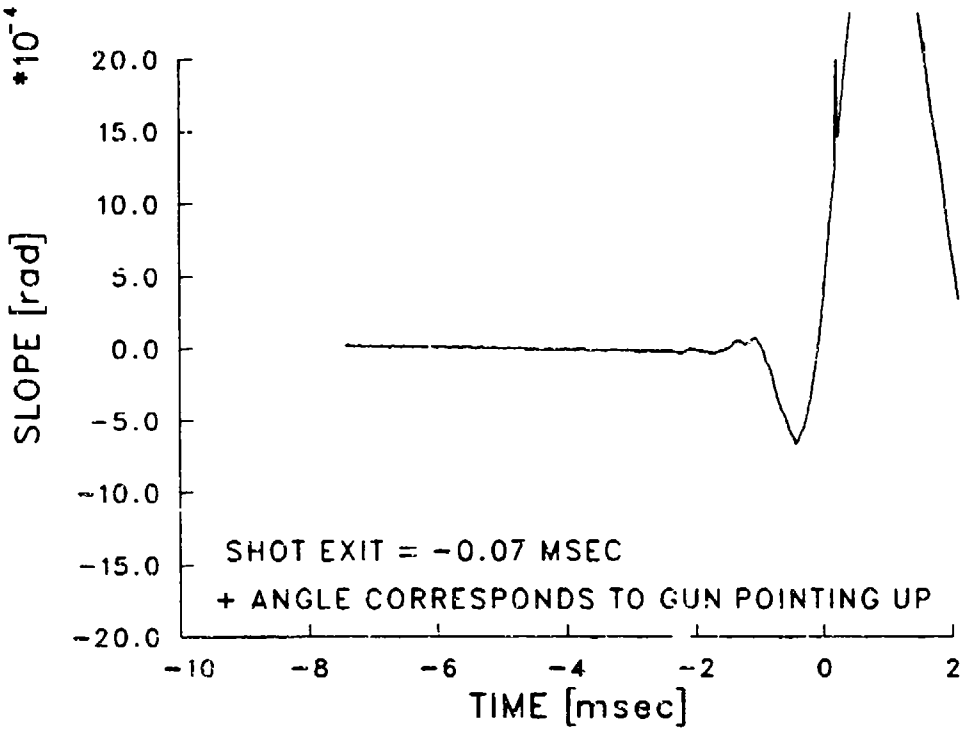

Figure 8b. Vertical muzzle pointing angle: APDS-T projectile.

Figure 9. Orthogonal x-ray array.

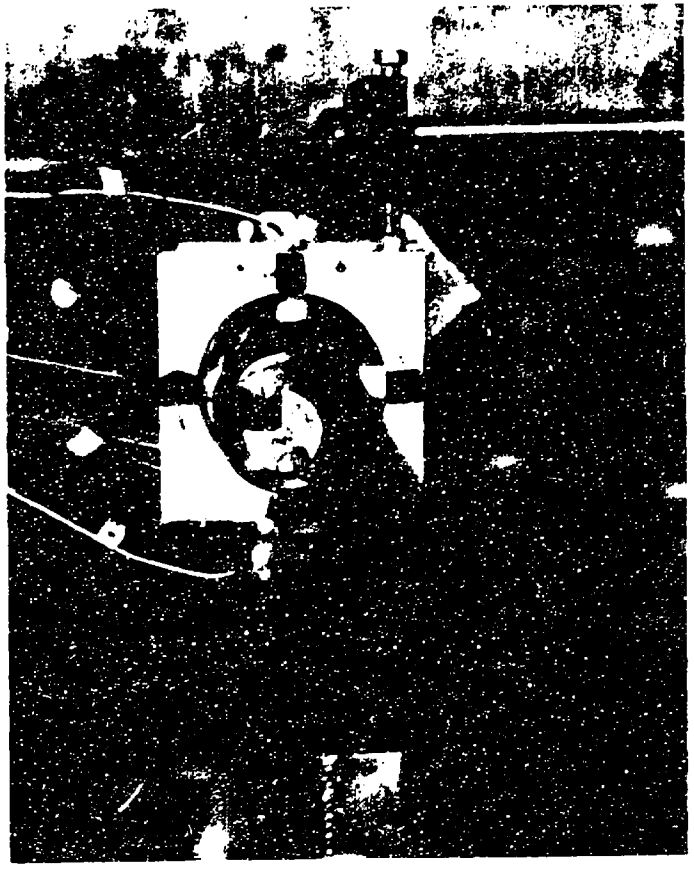

Figure 10. Muzzle and fiducial cable.

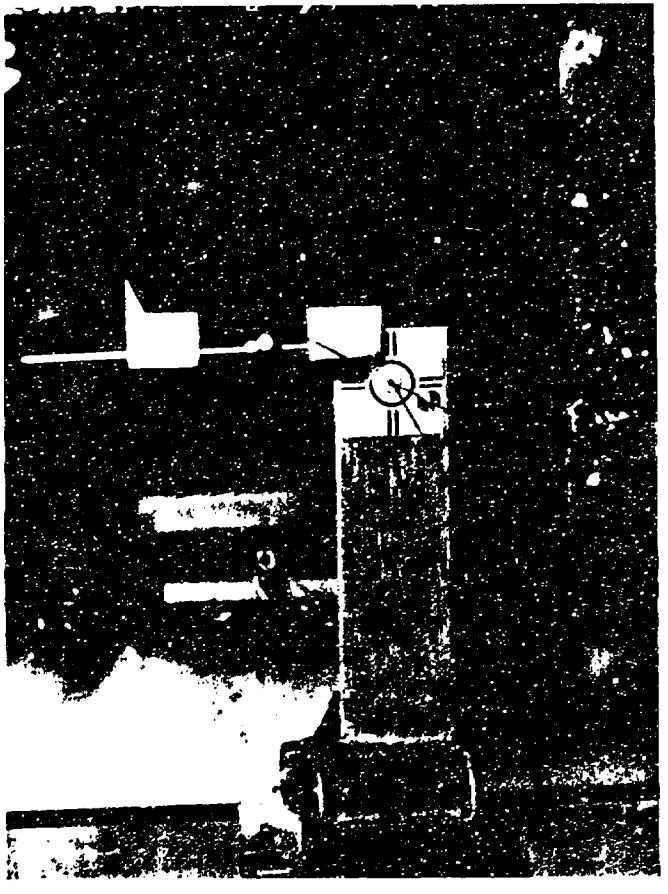

Figure 11. Downrange target and fiducial cable.

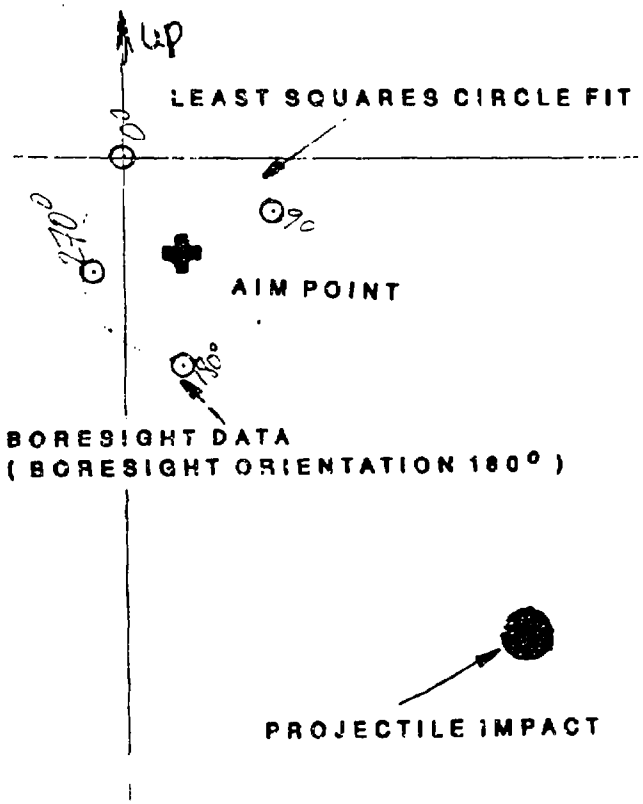

Figure 12. Boresight collimation on target.

Figure 13. Line-of-fire sighting sphere.

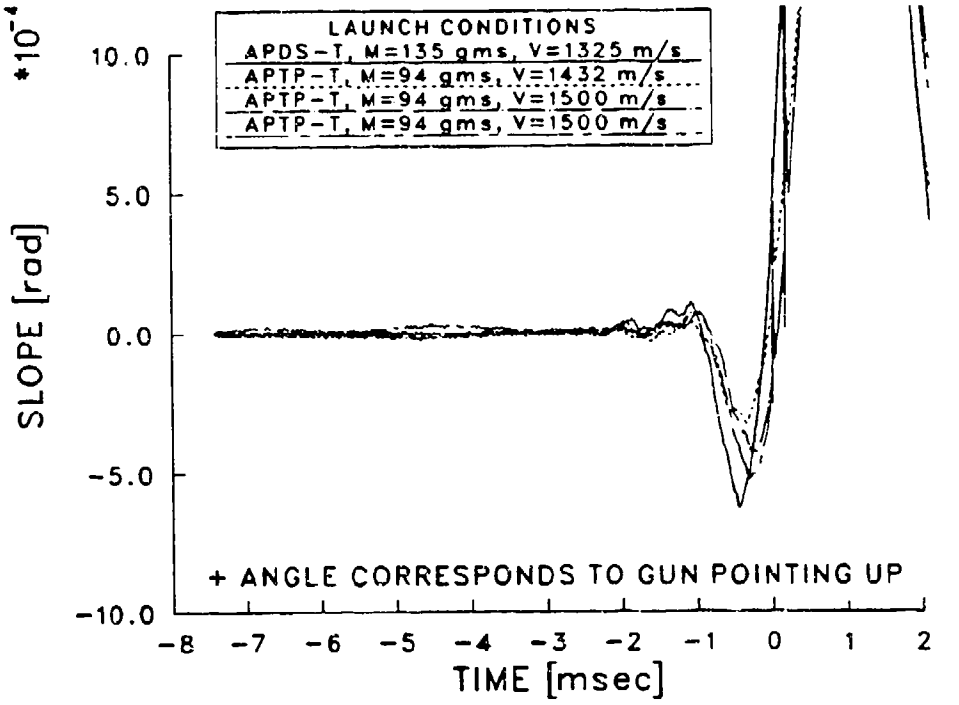

Figure 14a. Vertical muzzle pointing angle.

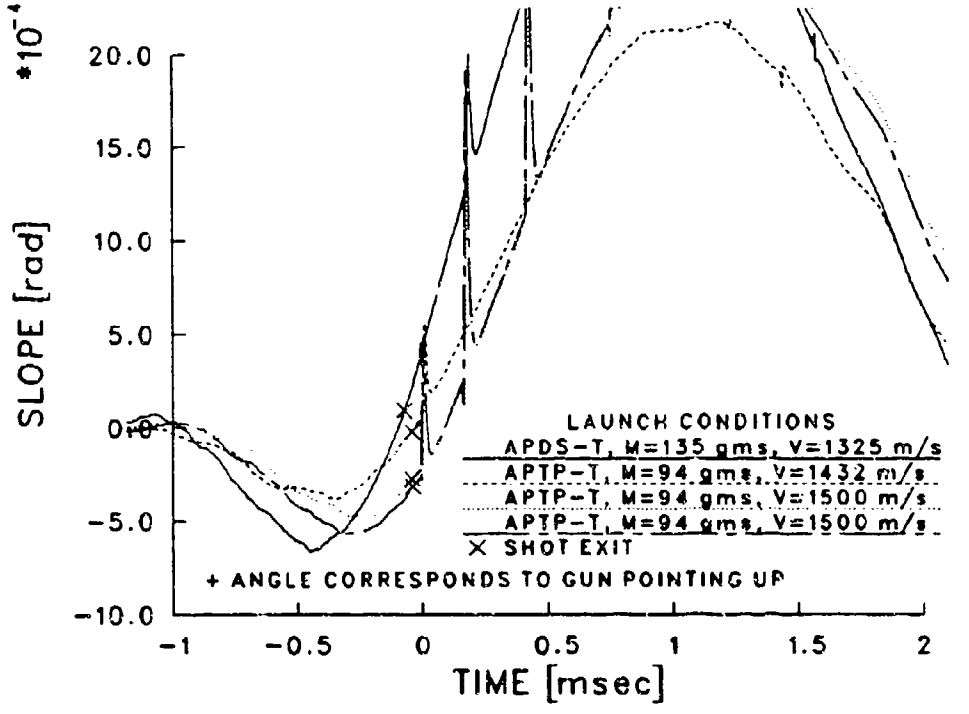

Figure 14b. Vertical muzzle pointing angle at shot exit.

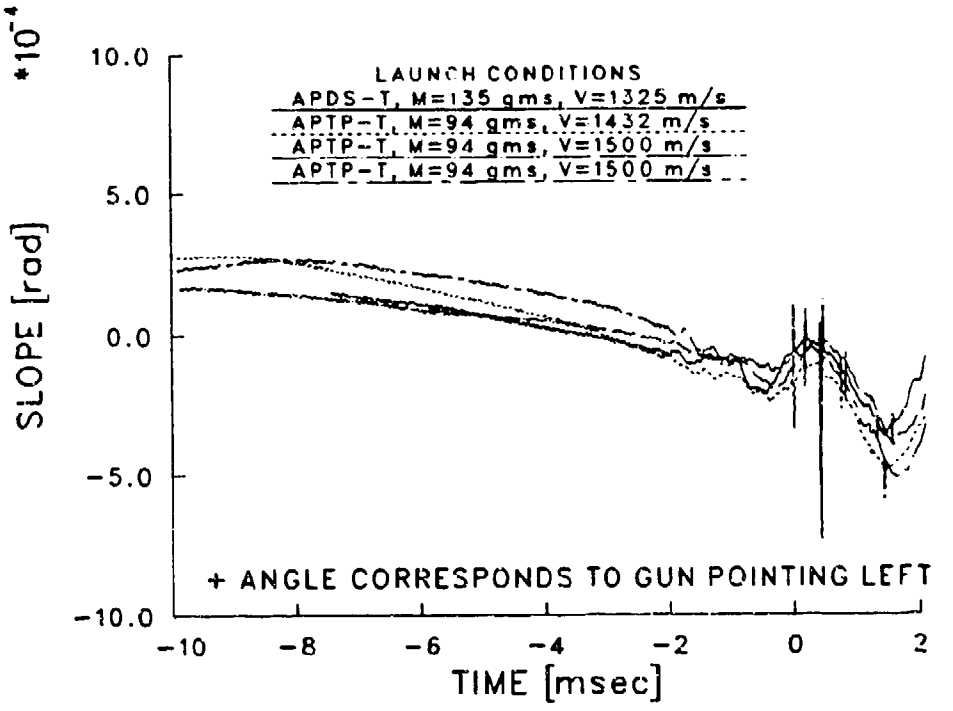

Figure 14c. Horizontal muzzle pointing angle.

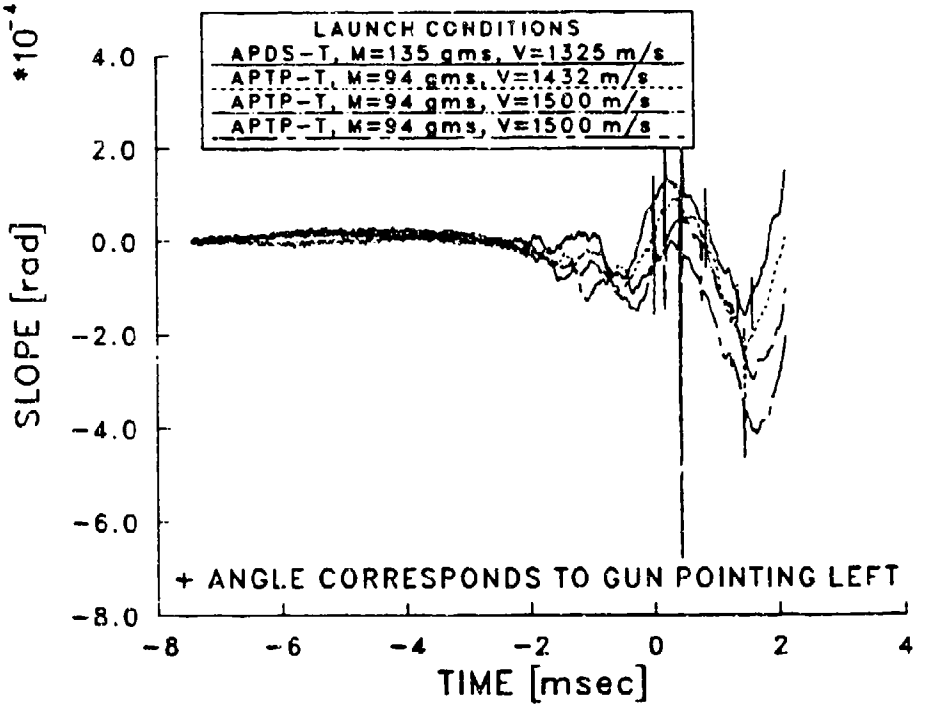

Figure 15. Corrected horizontal muzzle pointing angle.

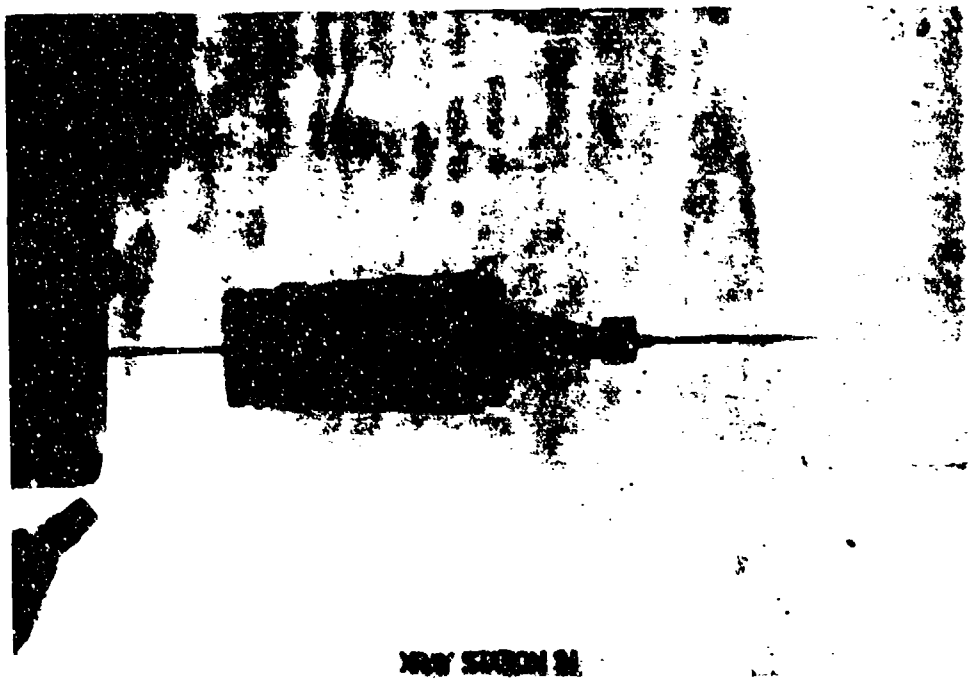

Figure 16a. Horizontal x-ray of APTP-T: station (1).

Figure 16b. Horizontal x-ray of APTP-T: station (2).

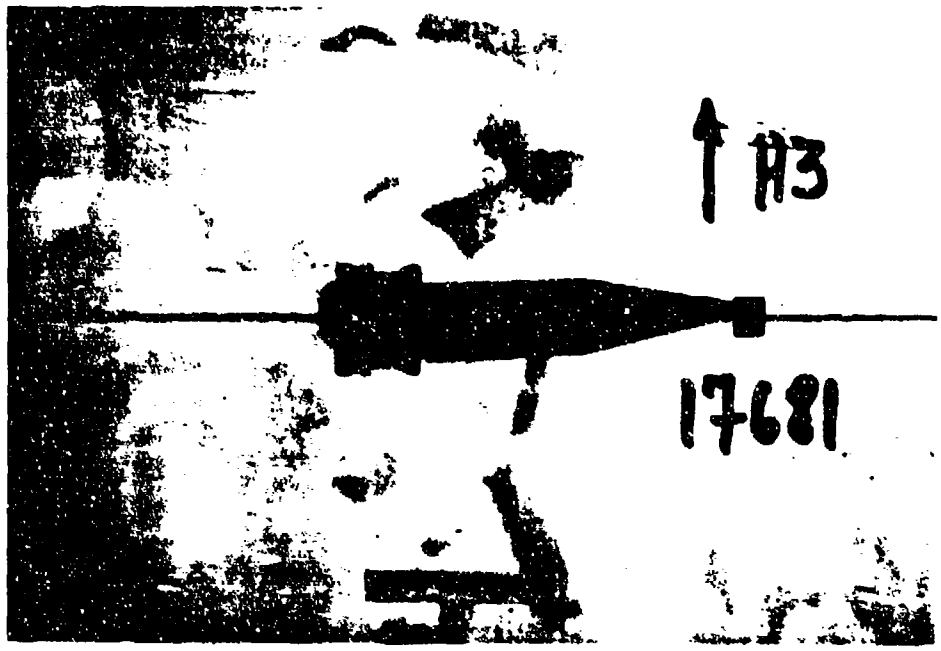

Figure 16c. Horizontal x-ray of APTP-T: station (3).

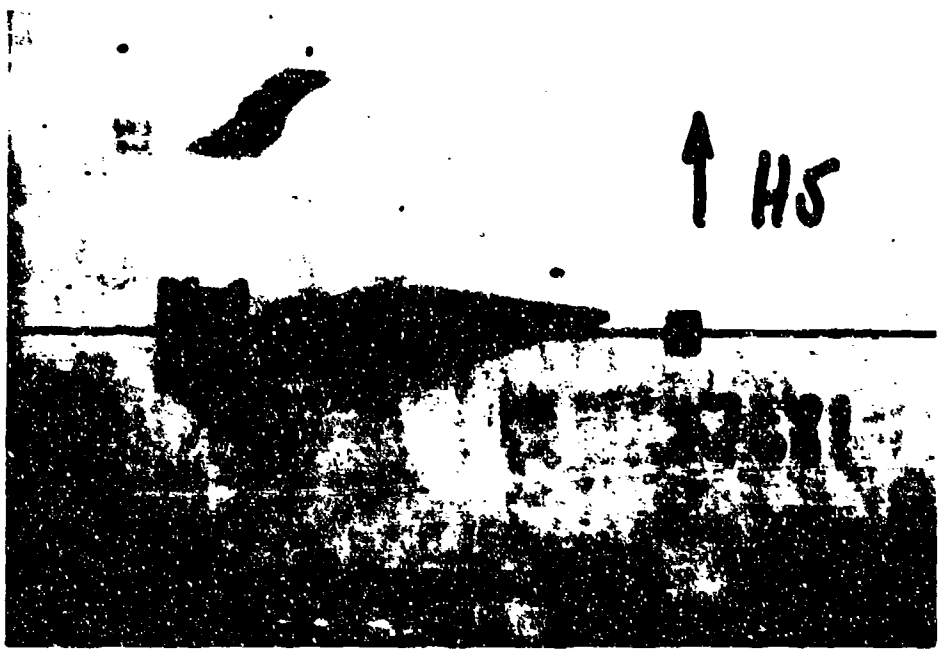

Figure 16d. Horizontal x-ray of APTP-T: station (4).

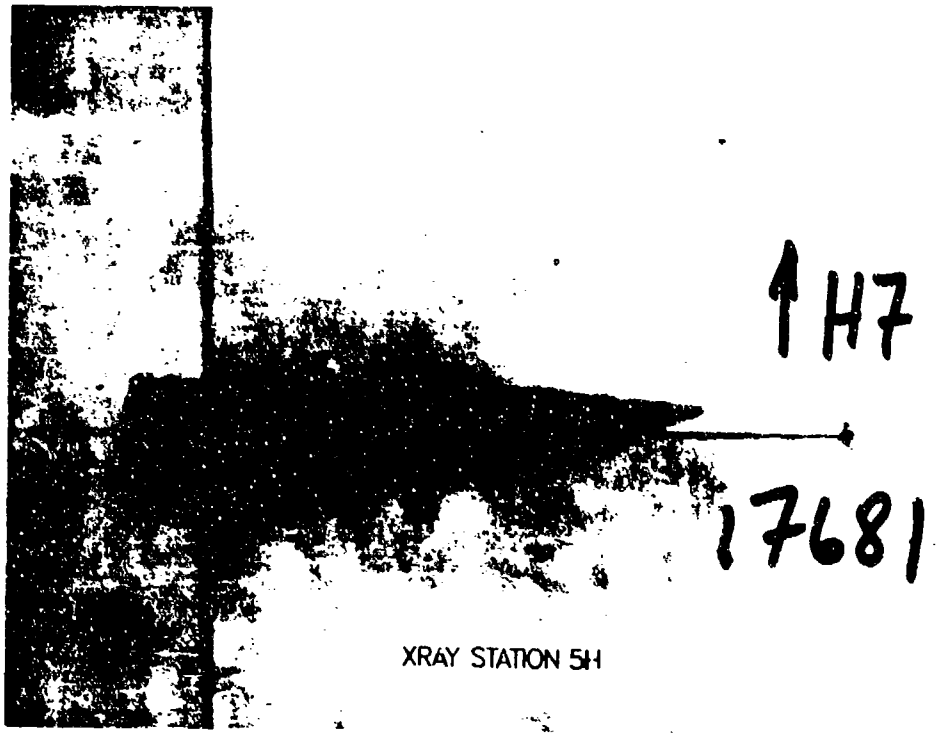

Figure 16e. Horizontal x-ray of APTP-T: station (5).

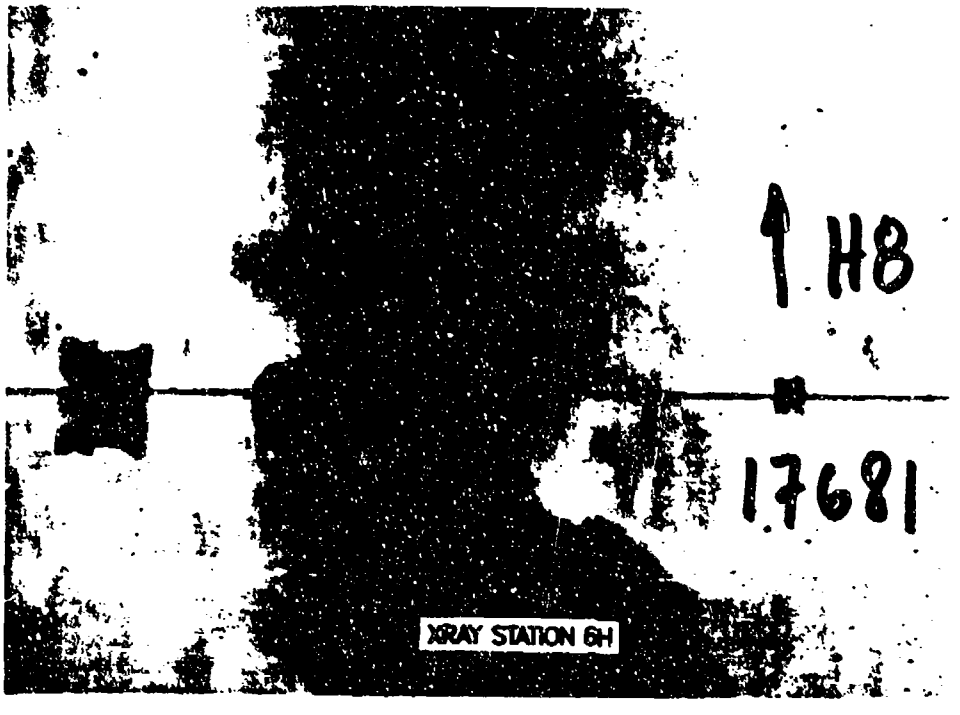

Figure 16f. Horizontal x-ray of APTP-T: station (6).

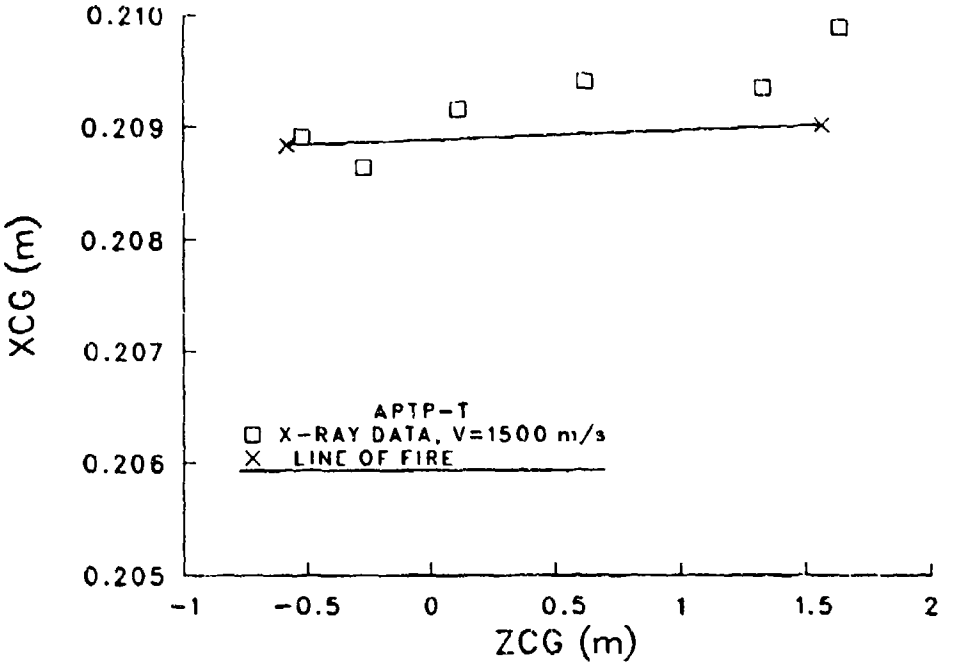

Figure 17a. Horizontal CG motion at the muzzle.

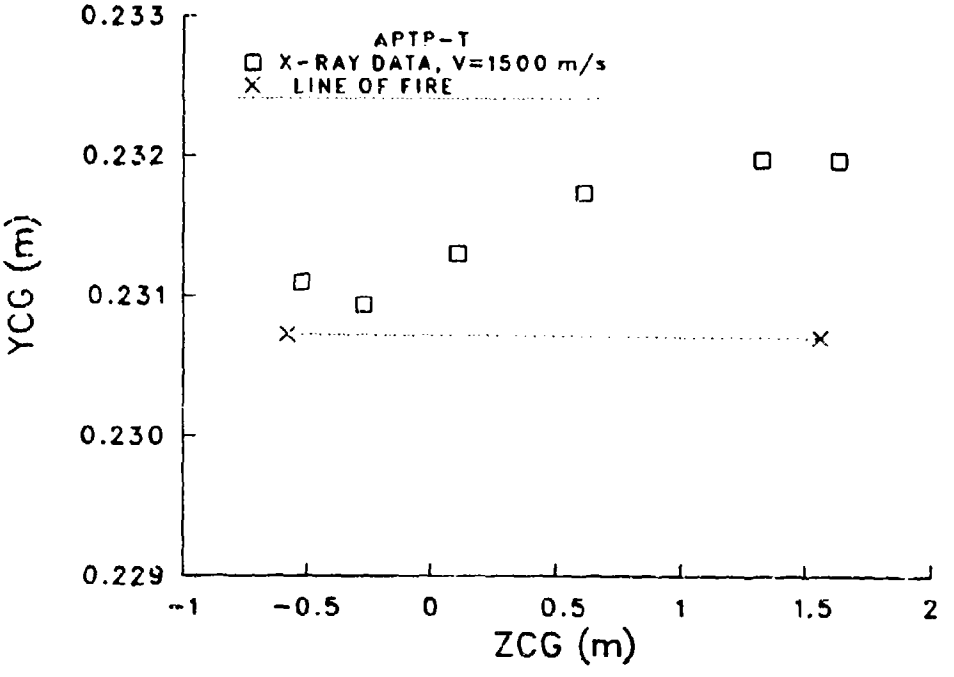

Figure 17b. Vertical CG motion at the muzzle.

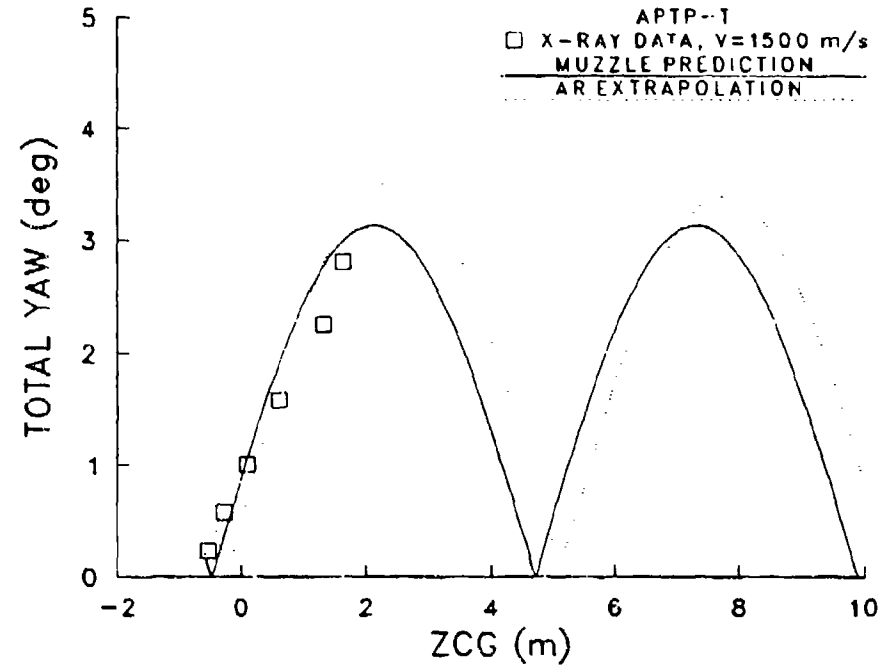

Figure 18a. Total yaw at the muzzle.

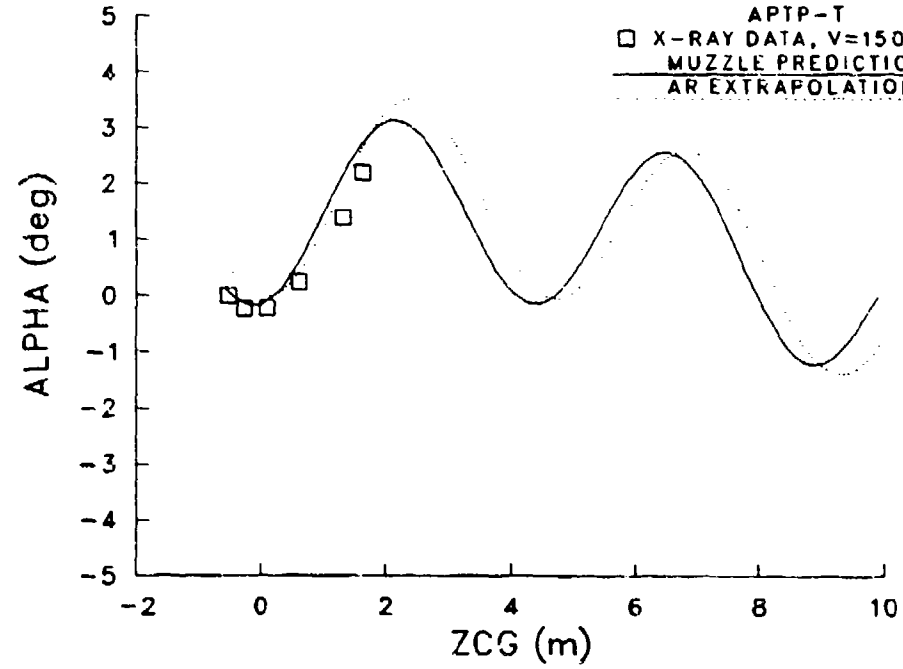

Figure 18b. Angle of attack at the muzzle.

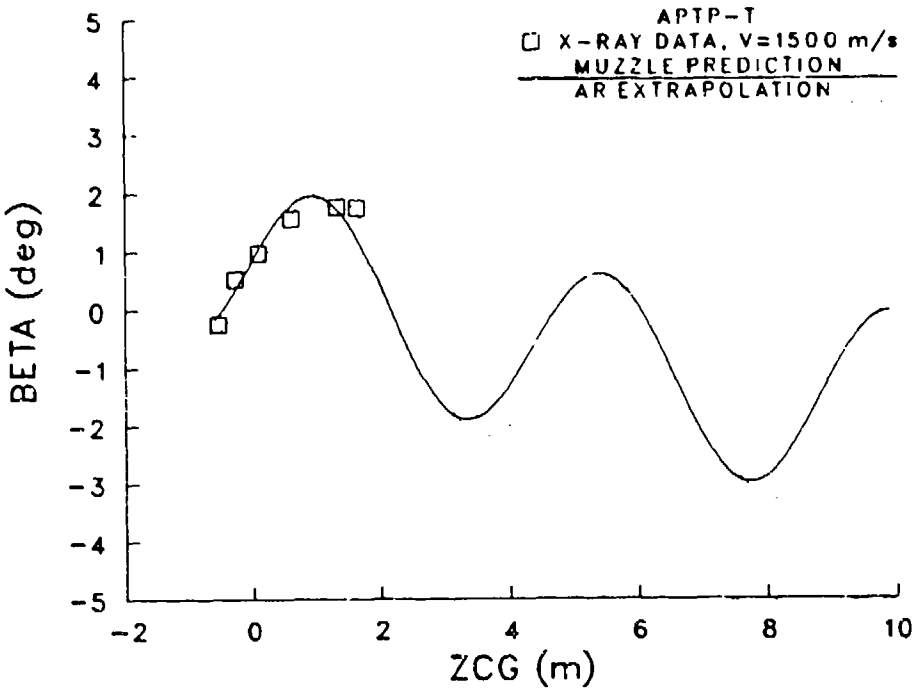

Figure 18c. Angle of sideslip at the muzzle.

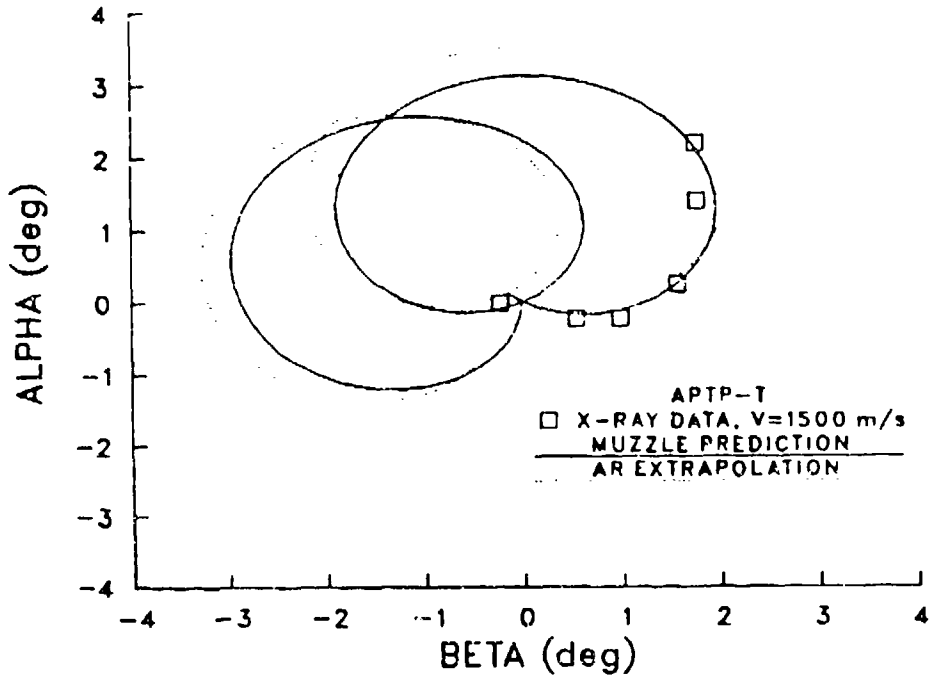

Figure 18d. Angle of attack vs. angle for sideslip at the muzzle.

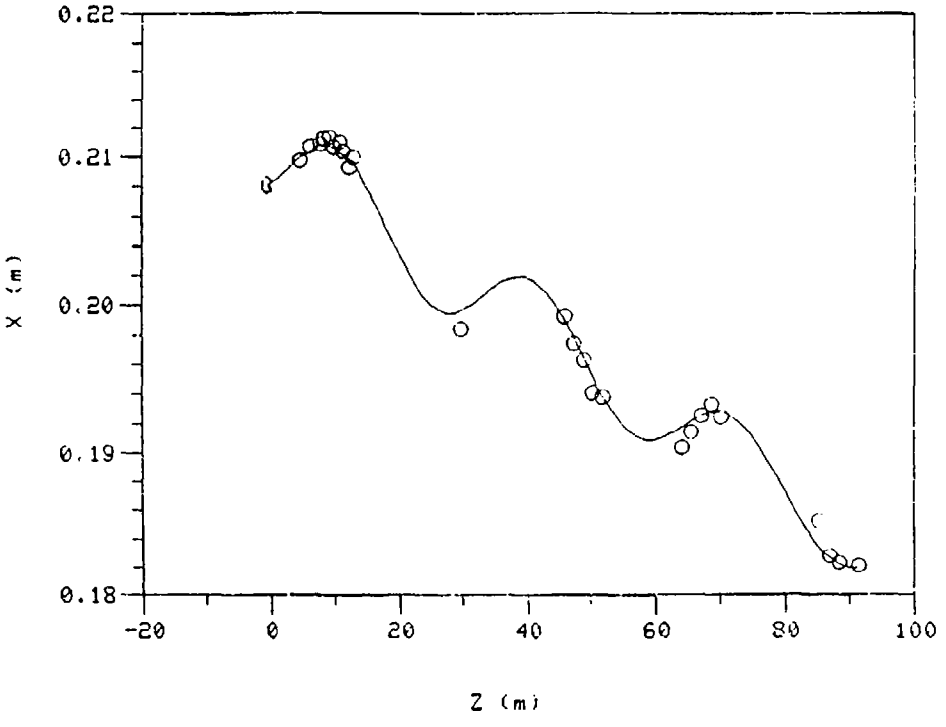

Figure 19a. Horizontal CG motion in the ARF.

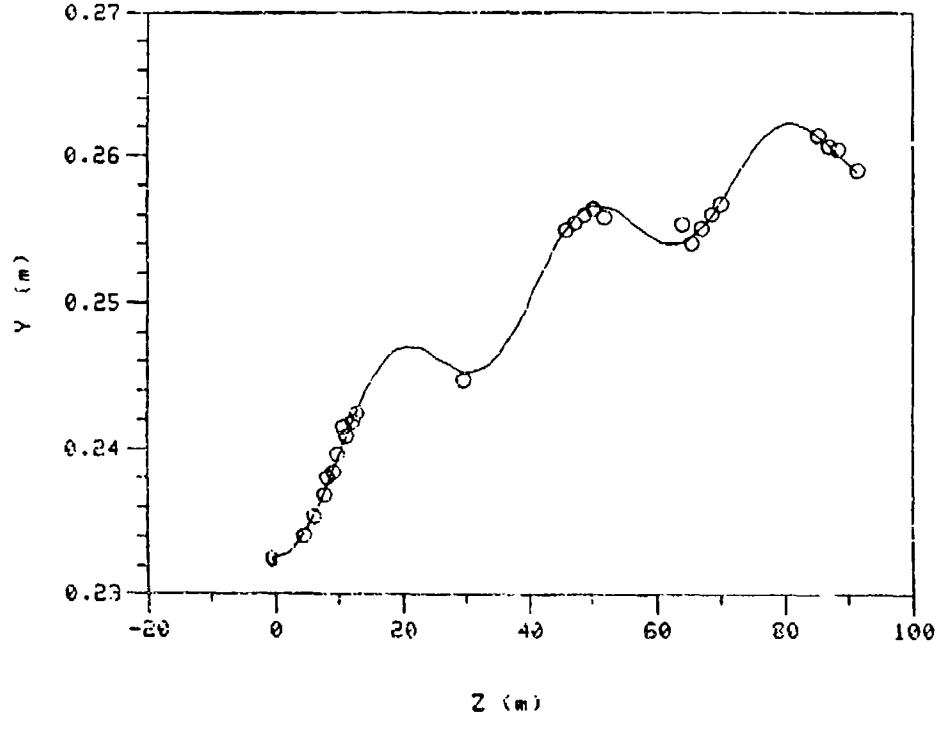

Figure 19b. Vertical CG motion in the ARF.

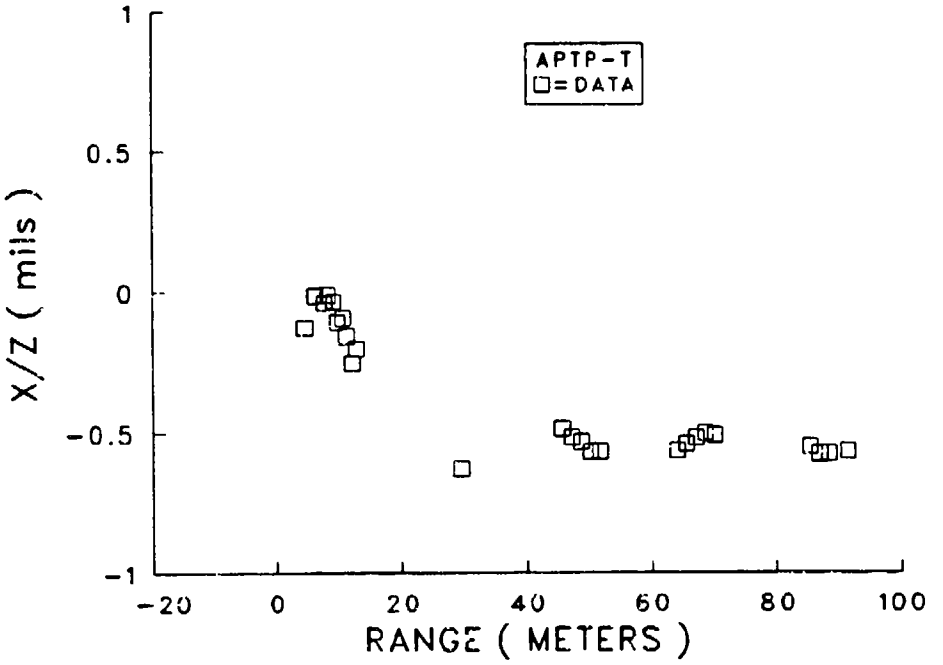

Figure 20. Horizontal aerodynamic jump in the ARF.

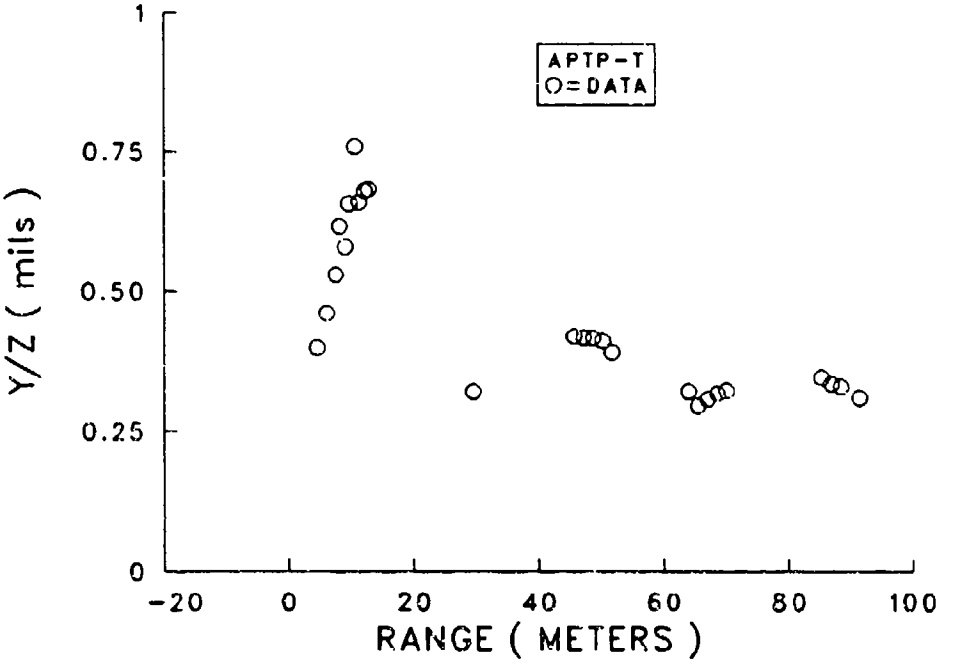

Figure 21. Vertical aerodynamic jump in the ARF.

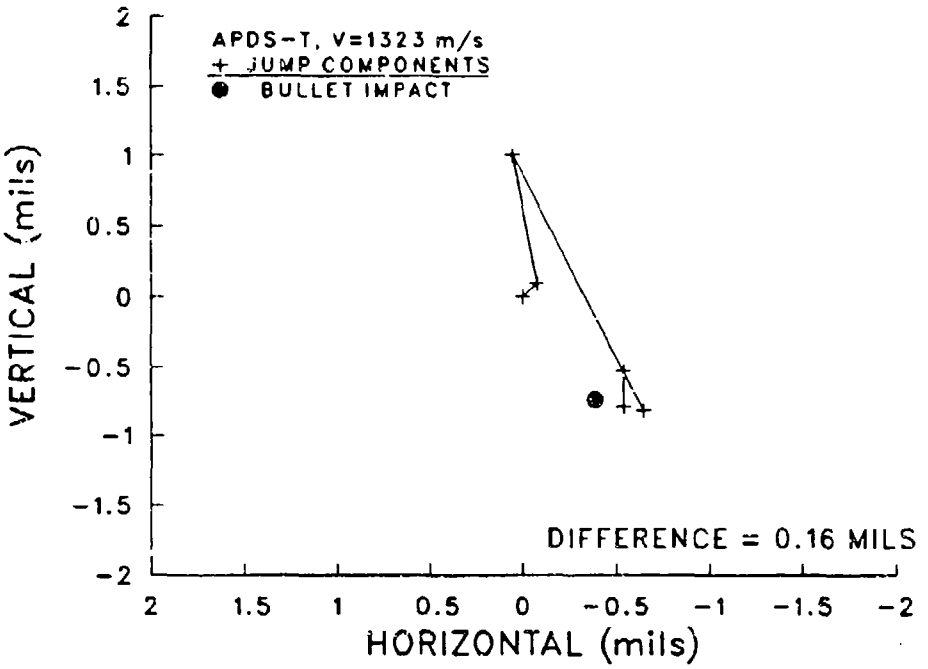

Figure 22. Jump components APDS-T projectile.

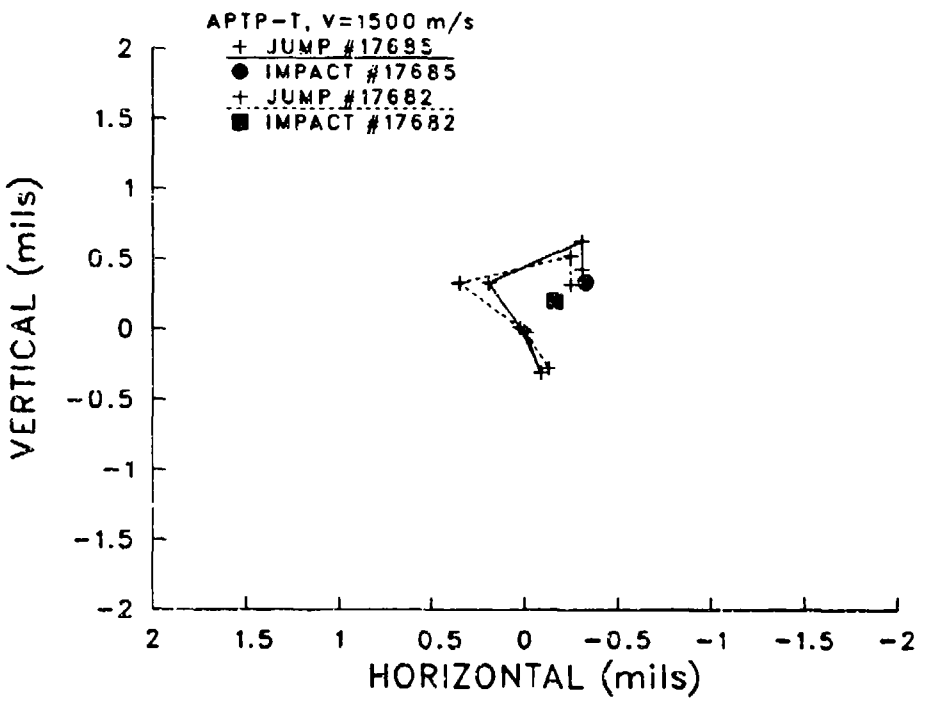

Figure 23. Jump components APTP-T projectile.

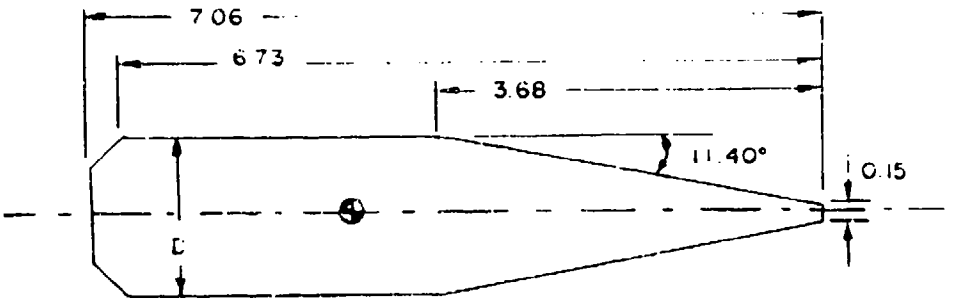

D = 1.65 cm
L/D = 4.28
M = 75.8 gm
I_x = 22.8 gm-cm^2
I_y = 183.0 gm-cm^2
V = 1500 m/s
X_{cg} = 4.52 cm (from the nose)

Figure 24. Monolithic steel APTP-T projectile.

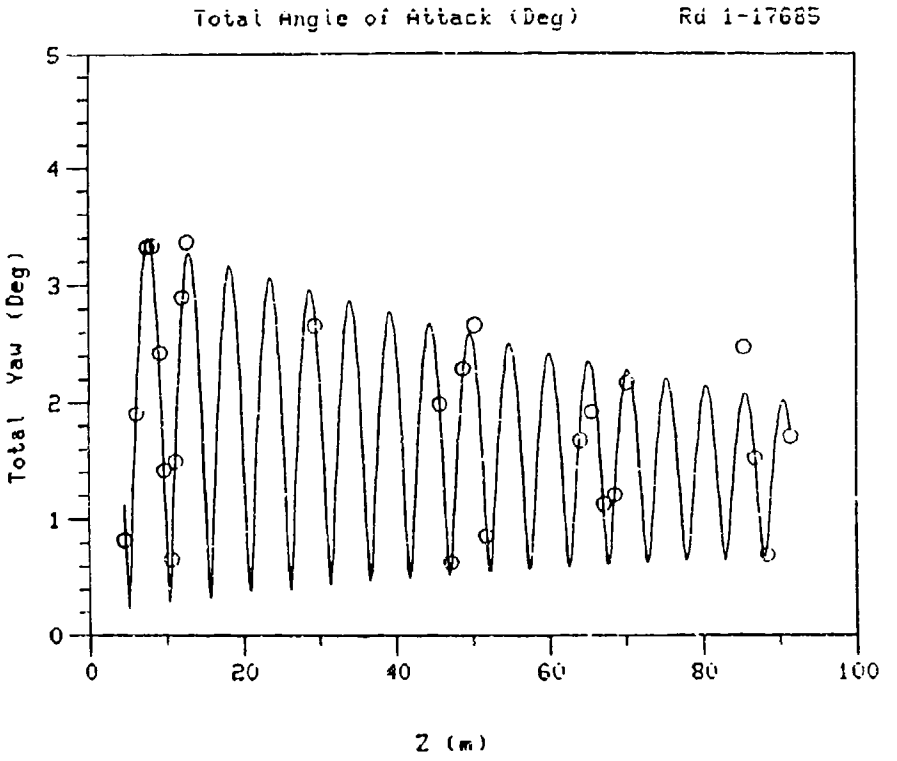

Figure 25a. Total Yaw measured in the ARF.

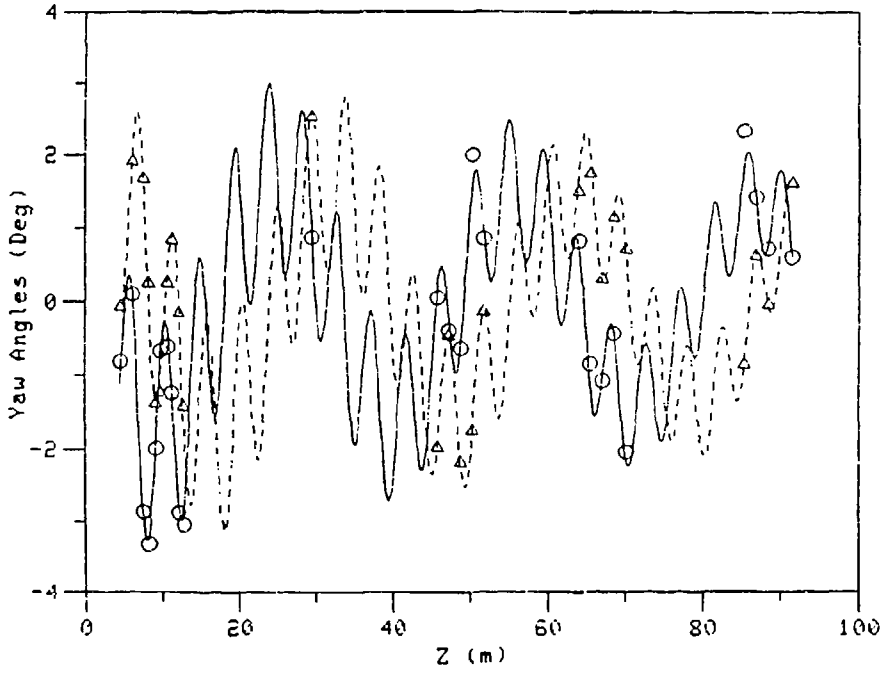

Figure 25b. Yaw components measured in the ARF.

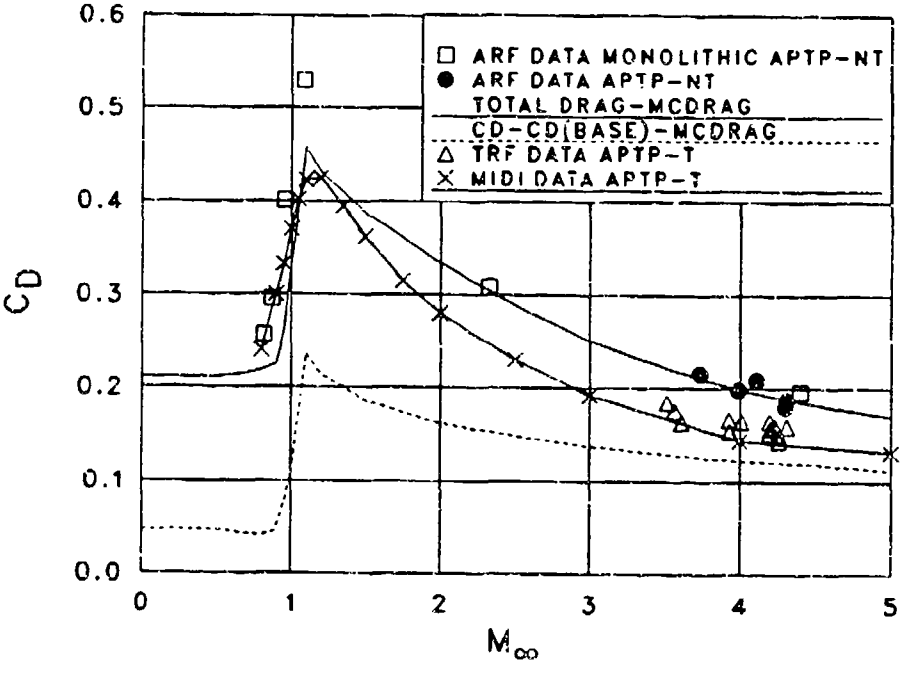

Figure 26. Drag vs. Mach number: APTP-T projectile.

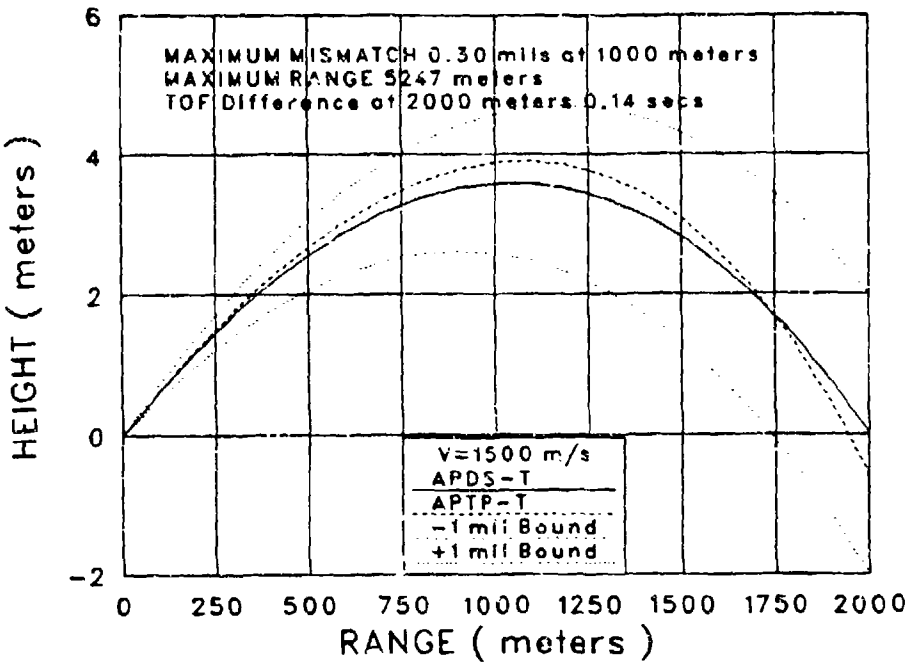

Figure 27. Ballistic match of the APTP-T and the APDS-T projectiles.

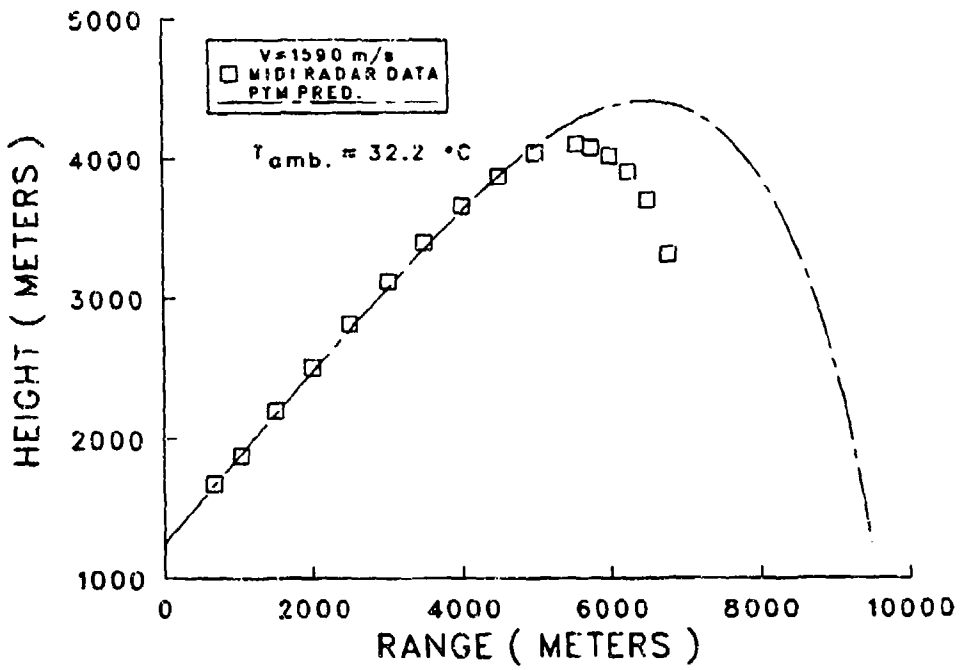

Figure 28a. Point mass trajectory: Ft. Bliss test conditions.

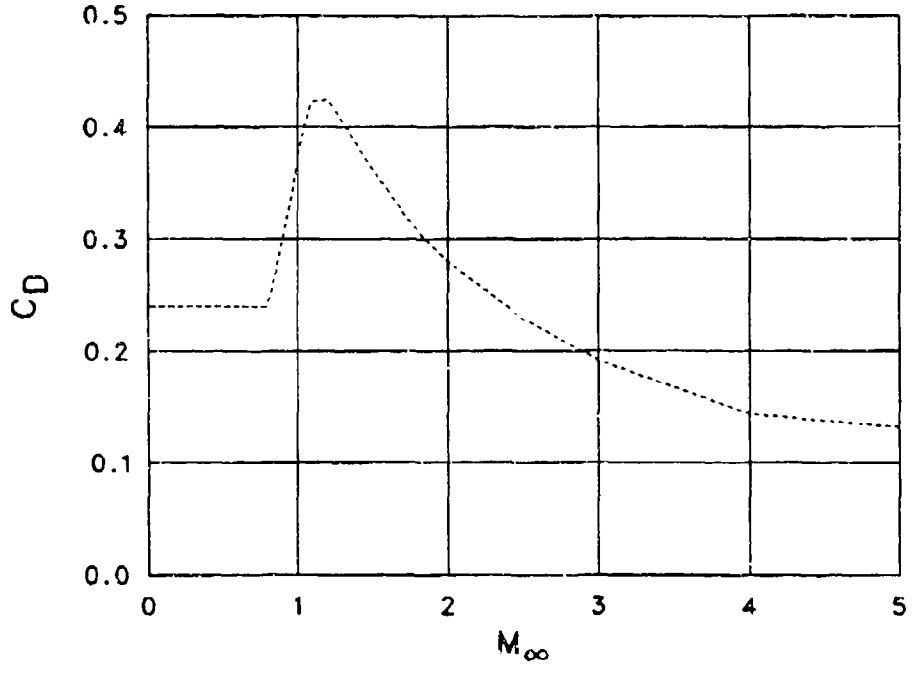

Figure 28b. Drag vs. Mach number for point mass trajectory prediction.

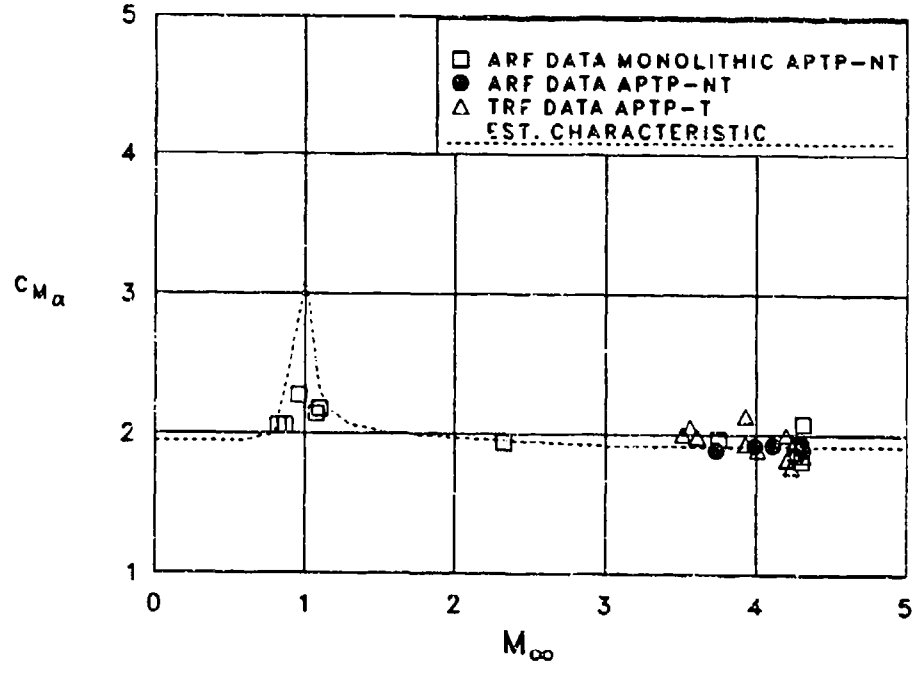

Figure 29a. Static moment coefficient: APTP-T projectile.

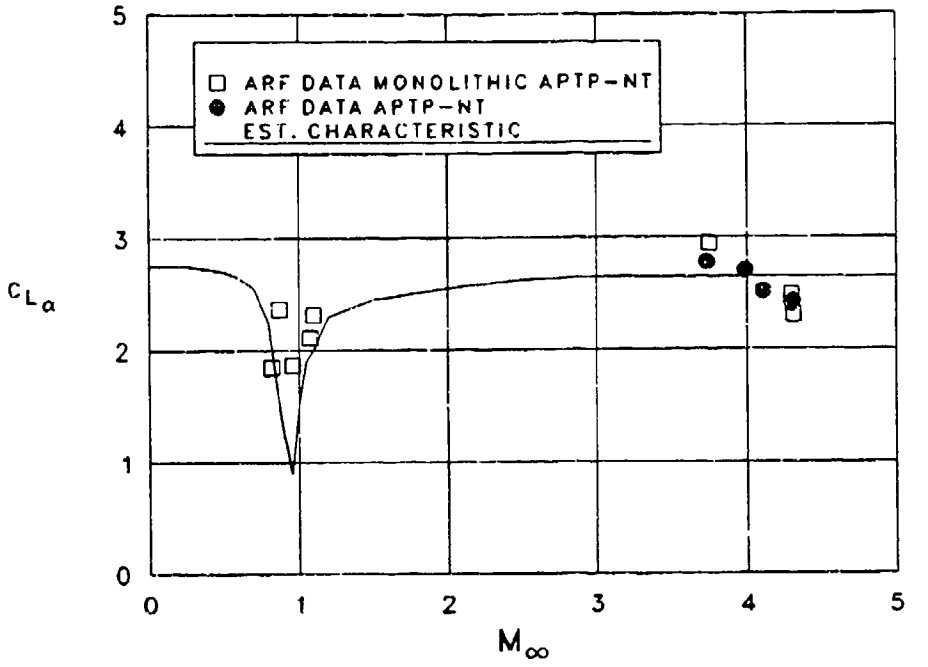

Figure 29b. Lift coefficient: APTP-T projectile.

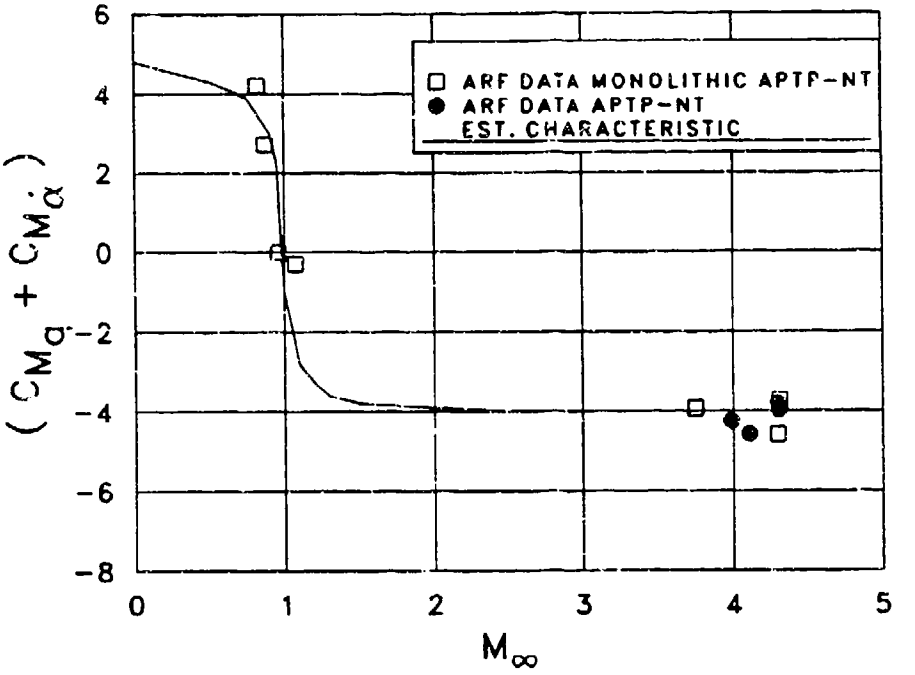

Figure 29c. Pitch damping moment coefficient: APTP-T projectile.

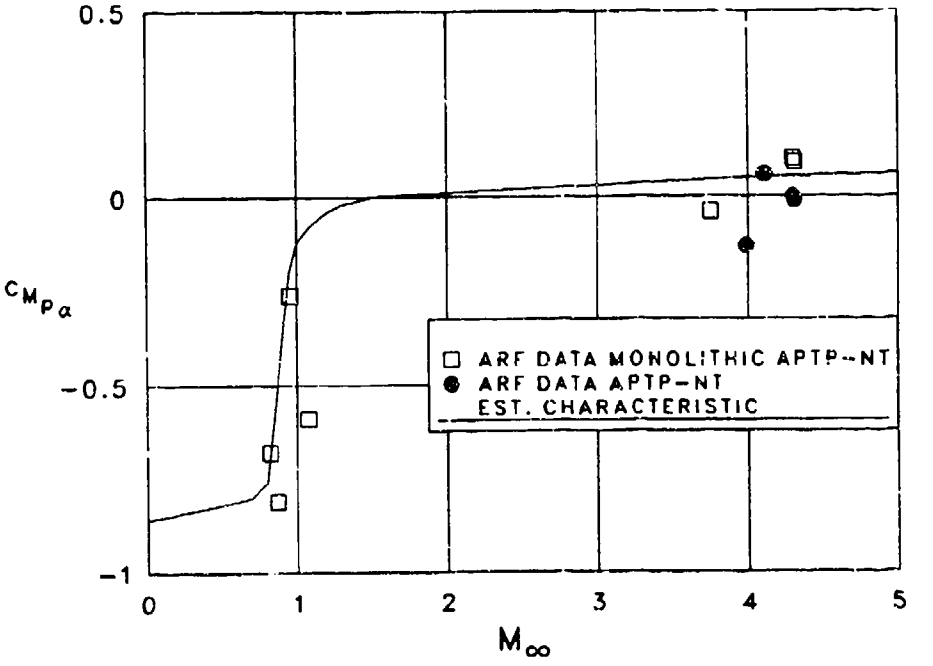

Figure 29d. Magnus moment coefficient: APTP-T projectile.

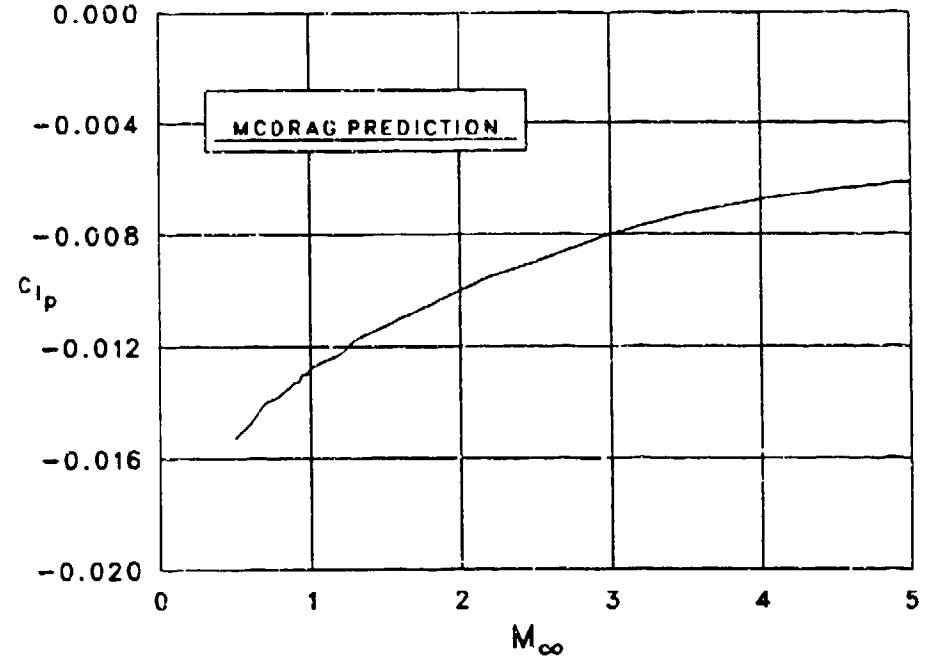

Figure 30. Roll damping coefficient: APTP-T projectile.

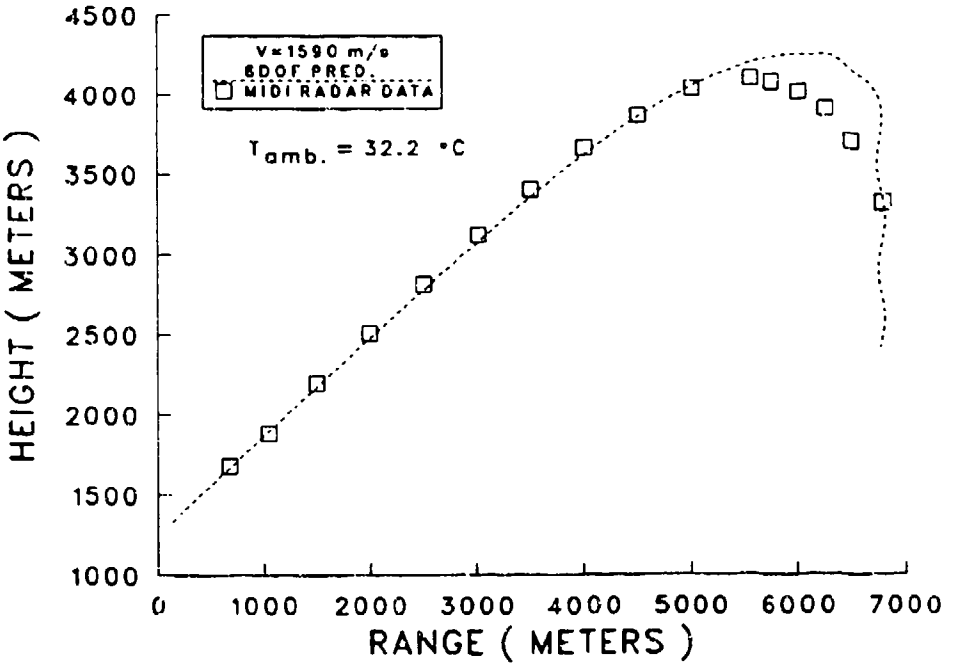

Figure 31a. Height vs. range: 6DOF prediction and radar data.

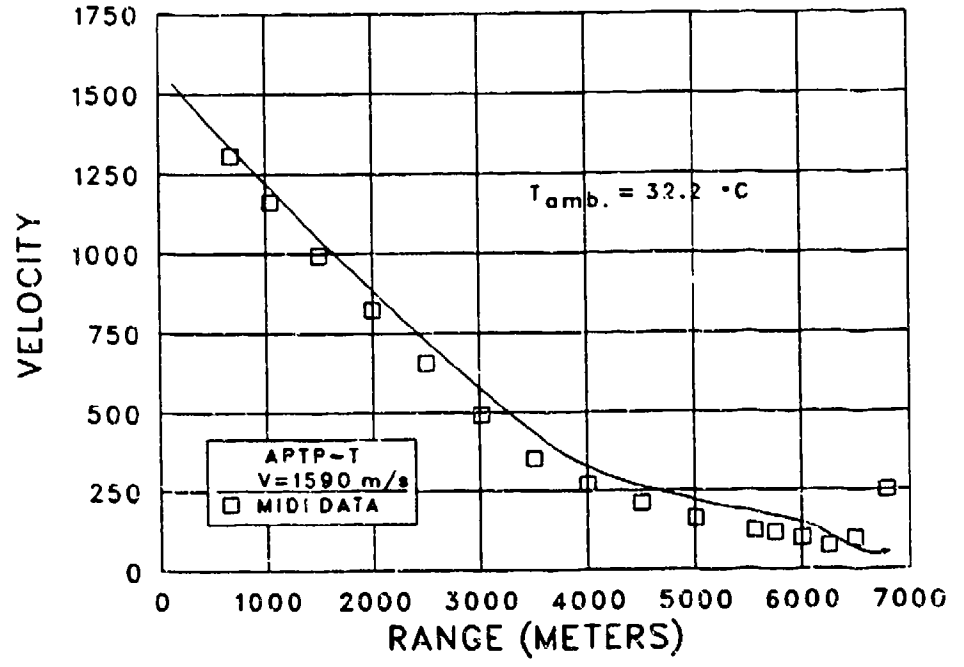

Figure 31b. Velocity vs. range: 6DOF prediction and radar data.

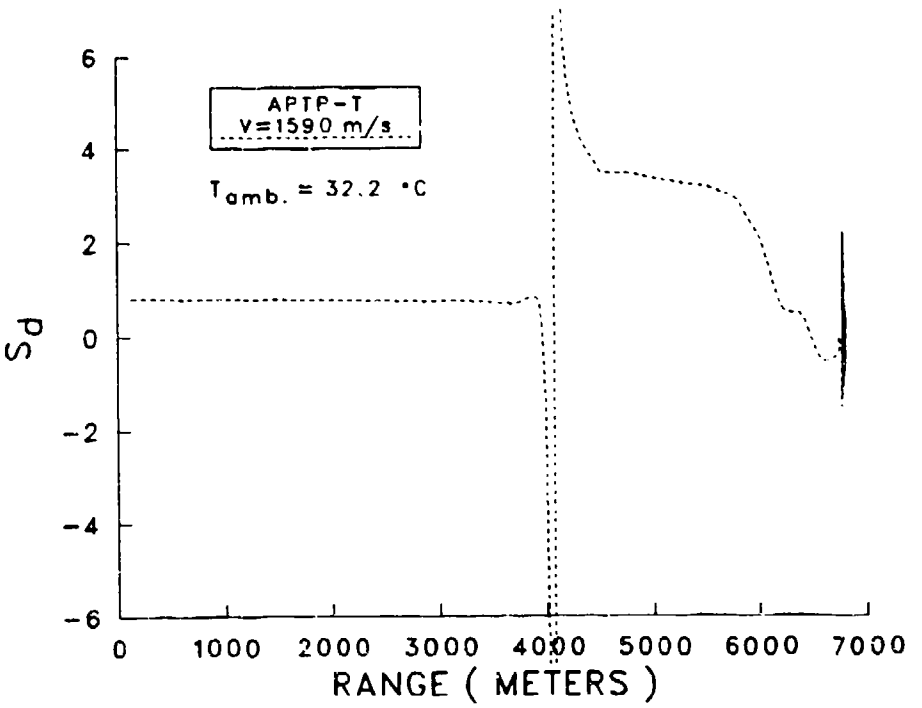

Figure 31c. Dynamic stability factor vs. range: 6DOF prediction.

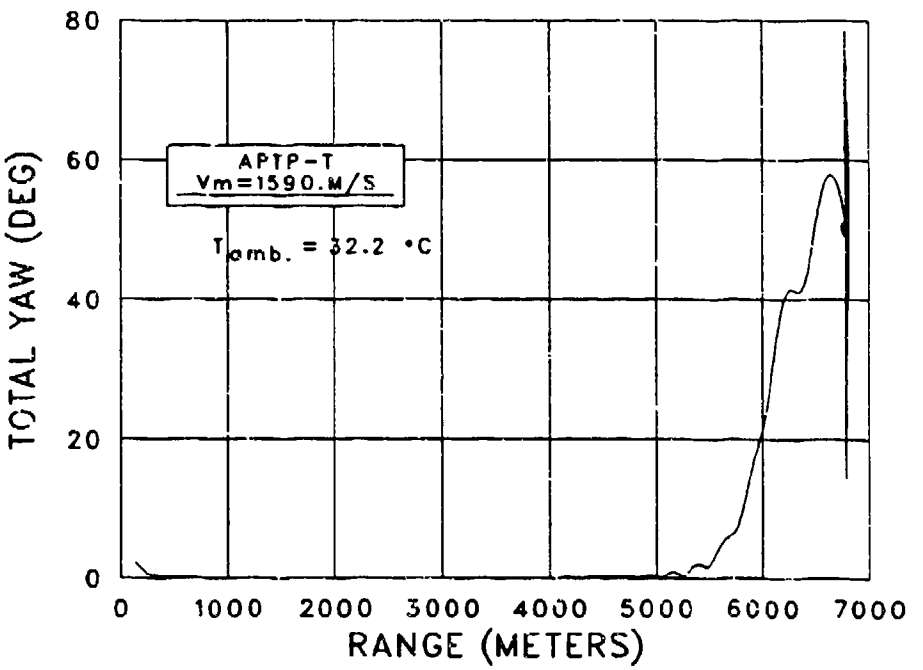

Figure 31d. Total Yaw vs. range: 6DOF prediction.

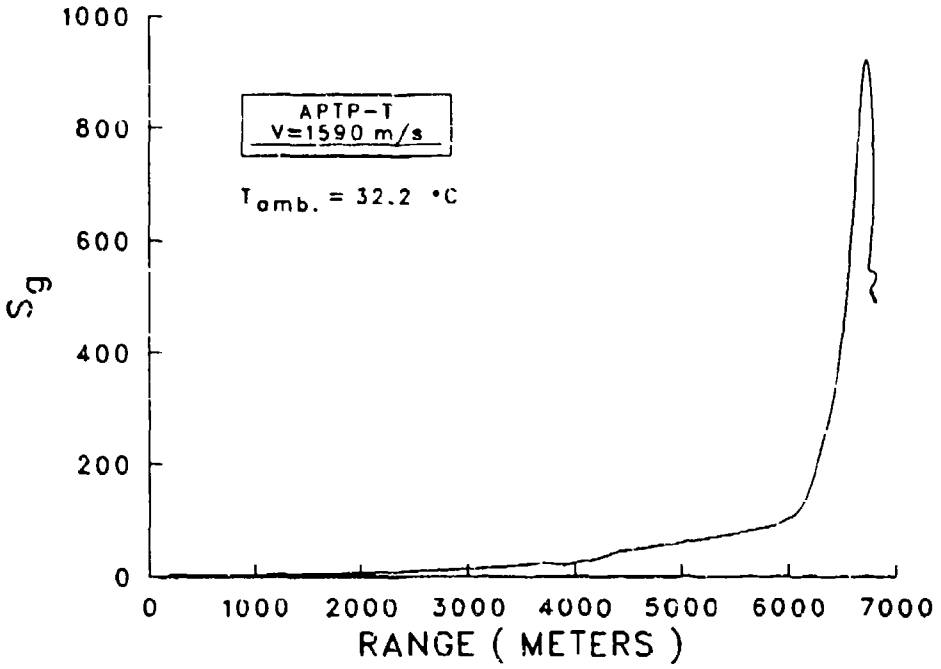

Figure 31e. Gyroscopic stability factor vs. range: 6DOF prediction.

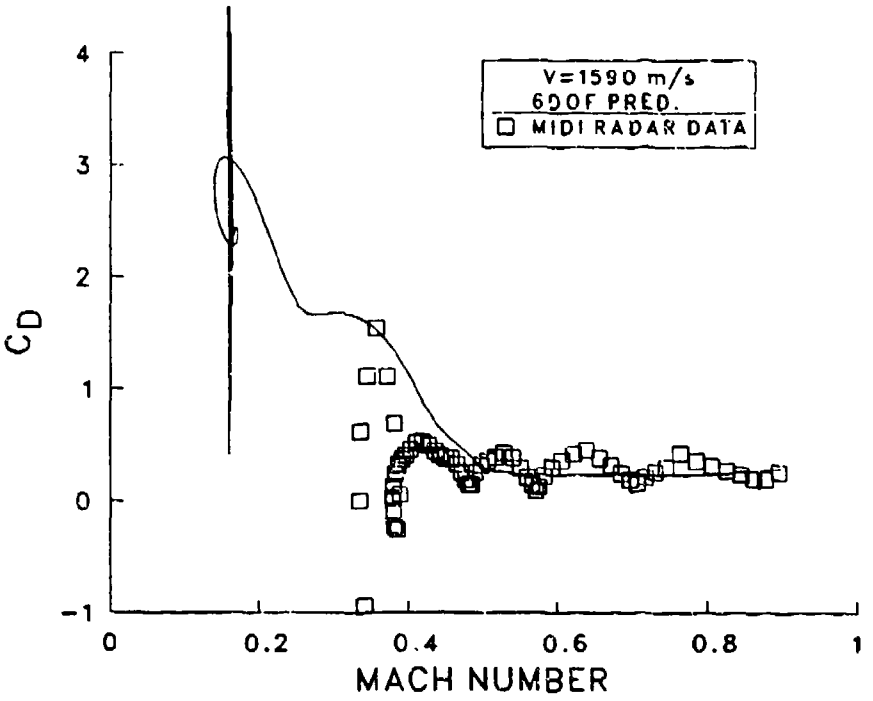

Figure 32. Total drag coefficient vs. subsonic Mach number: 6DOF prediction and radar data.

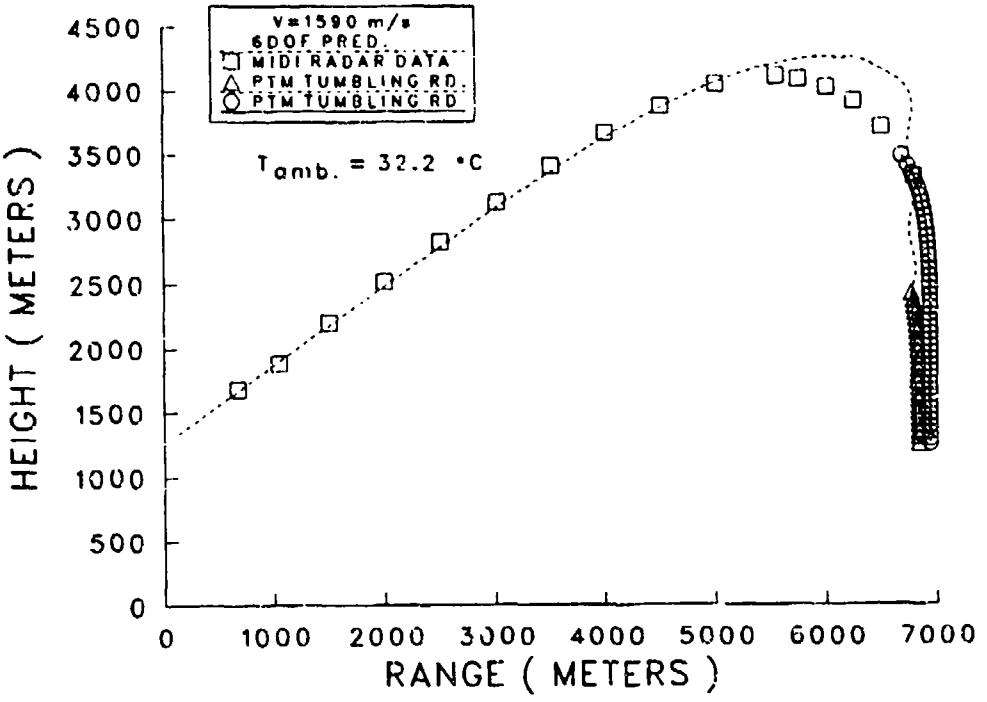

Figure 33. Trajectory extrapolation to the ground plane.

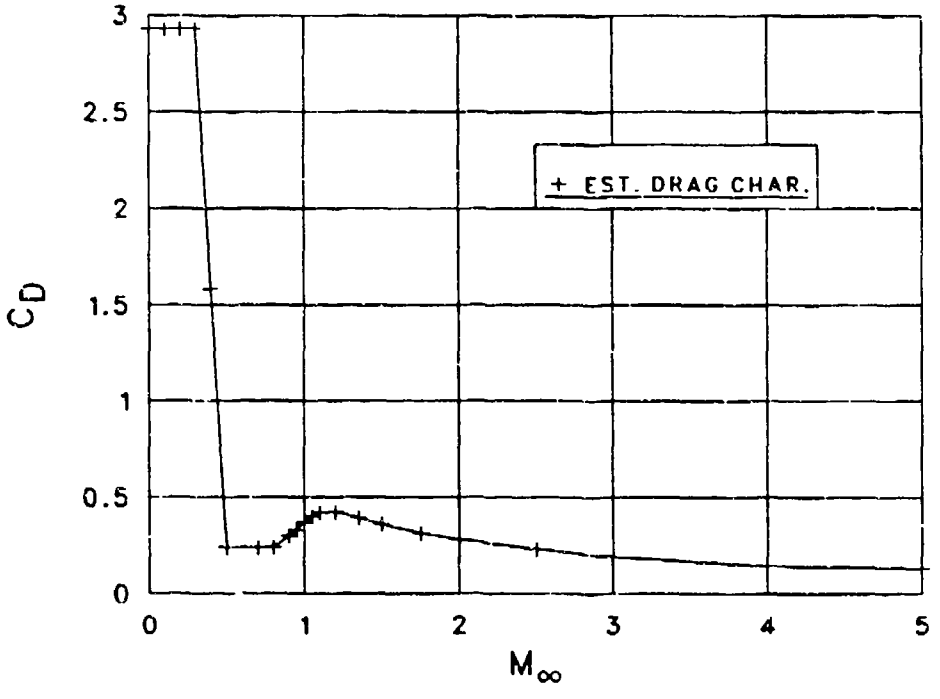

Figure 34. Drag vs. Mach number: APTP-T projectile.

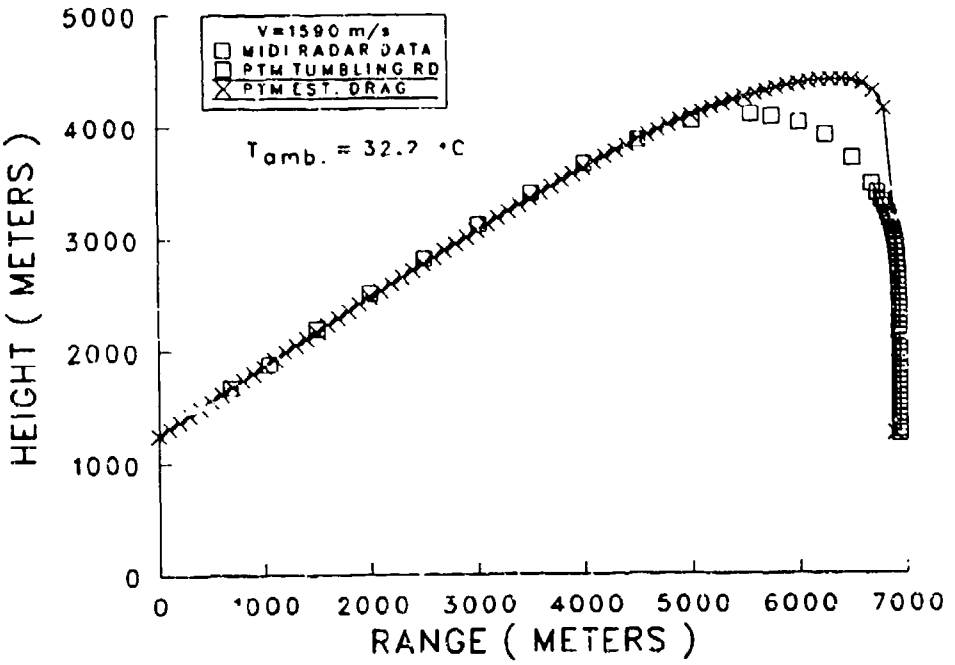

Figure 35. Interim point mass trajectory compared to radar data: Ft. Bliss test conditions.

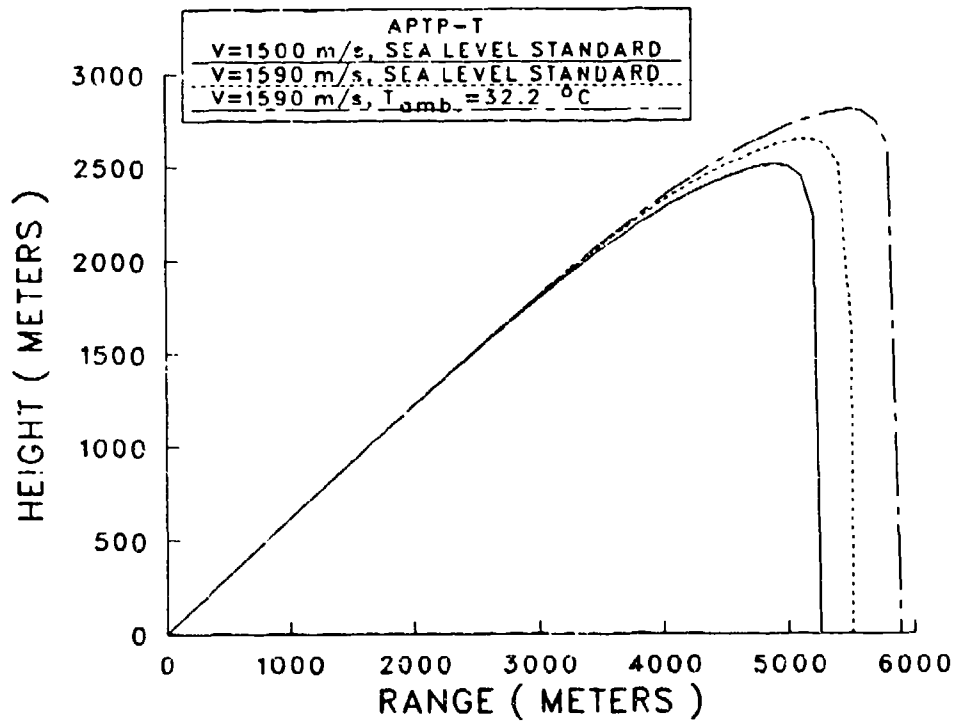

Figure 36. Sea level trajectory predictions.

REFERENCES

1. Celmins, I., "Aerodynamic Characteristics of Fin and Flare Stabilized 25MM Training Round Prototypes," Proceedings of the Tenth International Symposium on Ballistics, San Diego, California, October 27-29, 1987, ADPA, 1700 North Moore Street, Arlington, Virginia 22209-1942.

2. Glotz, G., Lecker, J., and Schilling, H., "Lochkegelleitwerk Aerodynamics," Proceedings of the Seventh International Symposium on Ballistics, The Hague, The Netherlands, 19-21 April 1983, ADPA, 1700 North Moore Street, Arlington, Virginia 22209-1942.

3. Biele, J.K., "Drag and Flow Field Characteristics of Two Complex-Shaped Projectile," Proceedings of the Seventh International Symposium on Ballistics, The Hague, The Netherlands, 19-21 April 1983, ADPA, 1700 North Moore Street, Arlington, Virginia 22209-1942.

4. Mermagen, W.H., "First Diagnostic Tests of a 75mm Solid Fuel Ramjet Tubular Projectile," ARBRL-MR-03283, U. S. Army Ballistic Research Laboratory, Aberdeen Proving Ground, Maryland, June 1983. AD A130598.

5. Politis, E., Kind, R.J., and Abdelhamid, A.N., "An Aero Prediction Method for Tubular Shapes at Supersonic Mach Numbers," Final Report, Contract No. 05SU.3229192, Center for Advanced Engineering and Design, Carleton University, Ottawa, Ontario, K1S5B6, September 1983.

6. Plostins, P., McCoy, R., Mirabelle, F. and Robbins, F., "Preliminary Evaluation of Training Round Concepts for 25mm APFSDS-T Ammunition," Tenth International Symposium on Ballistics, San Diego, California October 27-29, 1987.

7. Murphy, C.H., "Free Flight Motion of Symmetric Missiles," BRL-TR-1216, U. S. Army Ballistic Research Laboratory, Aberdeen Proving Ground, Maryland, July 1963. (AD 442757)

8. Murphy, C.H., "Data Reduction for the Free Flight Spark Ranges," BRL-R-900, U. S. Army Ballistic Research Laboratory, Aberdeen Proving Ground, Maryland, February 1954. (AD 35833)

9. Bornstein, J., "Application of Proximity Sensors for Determination of Gun Tube Motion," Proceedings of the 33rd International Instrumentation Symposium, Las Vegas, Nevada, May 3-8, 1987, Paper #87-0282.

10. Schmidt, E.M., Plostins, P. and Bundy, M.L., "Flash Radiographic Diagnostics of Projectile Launch from Cannon," Proceedings of the 1984 Flash X-Ray Symposium, Denver, Colorado, May 22-24, 1984.

11. Schmidt, E.M., and Shear, D.D., "Aerodynamic Interference During Sabot Discard," BRL-R-1810, U. S. Army Ballistic Research Laboratory, Aberdeen Proving Ground, Maryland, August 1985. (AD B006781)

12. Plostins, P., "Launch Dynamics of APFSDS Ammunition," BRL-TR-2595, U. S. Army Ballistic Research Laboratory, Aberdeen Proving Ground, Maryland, October 1984. (AD A147374)

13. McCoy, R.L., "McDrag-A Computer Program for Estimating the Drag Coefficients of Projectiles," BRL-TR-02293, U. S. Army Ballistic Research Laboratory, Aberdeen Proving Ground, Maryland, February 1981. (AD 098110)

14. Dunn, D.J. Jr. and Porter W.R., "Air Drag Measurements of Fragments," BRL-MR-915, U. S. Army Ballistic Research Laboratory, Aberdeen Proving Ground, Maryland, August 1955. (AD 77240)

LIST OF SYMBOLS*

c	Ballistic Coefficient M/D^2
C	Propellant Mass
C_D	Drag Coefficient
C_{L_α}	Lift Coefficient
C_{ℓ_p}	Roll Damping Coefficient
C_{M_α}	Static Moment Coefficient
$C_{M_{p_\alpha}}$	Magnus Moment Coefficient
$C_{M_q} + C_{M_{\dot{\alpha}}}$	Pitch Damping Moment Coefficient
D	Projectile Diameter
I	Impulse
I_x	Axial Moment of Inertia
I_y	Transverse Moment of Inertia
L	Projectile Length
M	Projectile Mass
S_d	Dynamic Stability Factor
S_g	Gyroscopic Stability Factor
$T_{amb.}$	Ambient Atmospheric Temperature
V	Projectile Velocity
$X_{cg.}$	Projectile Center of Gravity Location
X	Horizontal Coordinate
Y	Vertical Coordinate
Z	Downrange Coordinate

* Aerodynamic coefficients conform with the definitions in Reference (7).

INTENTIONALLY LEFT BLANK.

DISTRIBUTION LIST

No. of Copies	Organization
12	Administrator Defense Technical Info Center ATTN: DTIC-FDAC Cameron Station, Bldg. 5 Alexandria, VA 22304-6145
1	HQDA DAMA-ART-M Washington, DC 20310
1	Commander US Army Materiel Command ATTN: AMCDRA-ST 5001 Eisenhower Avenue Alexandria, VA 22333-0001
1	Director US Army Aviation Research and Technology Activity Ames Research Center Moffett Field, CA 94035-1099
1	Commander US Army Communications - Electronics Command ATTN: AMSEL-ED Fort Monmouth, NJ 07703-5301
1	Commander CECOM R&D Technical Library ATTN: AMSEL-IM-L (Reports Section) B.2700 Fort Monmouth, NJ 07703-5000
1	Commander U.S. Army Missile Command Research, Development, and Engineering Center ATTN: AMSMI-RD Redstone Arsenal, AL 35898-5230
1	Commander US Army Missile and Space Intelligence Center ATTN: AIAMS-YDL Redstone Arsenal, AL 35898-5000

No. of Copies	Organization
1	Commander US Army Tank Automotive Command ATTN: AMSTA-TSL Warren, MI 48397-5000
1	Commander US Army Armament Munitions & Chemical Command ATTN: AMSMC-IMP-L Rock Island, IL 61299-7300
8	Commander Armament RD&E Center US Army AMCCOM ATTN: SMCAR-MSI SMCAR-CCL-CA, Peter O'Neill Carol Ann Miller E. Malatesta R. Cickurs J. Hirlinger ATTN: SMCAR-AET-A, G. Fleming Dover, NJ 07801-5001
1	Commander Armament RD&E Center US Army AMCCOM ATTN: SMCAR-TDC Dover, NJ 07801-5001
1	Commander U.S. AMCCOM ARDEC CCAC Benet Weapons Laboratory ATTN: SMCAR-CCB-TL Watervliet, NY 12189-4050
1	Commandant US Army Infantry School ATTN: ATSH-CD-CS-OR Ft. Benning, GA 31905-5400
1	Commander US Army Development and Employment Agency ATTN: MODE-ORO Fort Lewis, WA 98433-5000

DISTRIBUTION LIST (continued)

No. of Copies	Organization
1	Director US Army TRADOC Analysis Center ATTN: ATOR-TSL White Sands Missile Range, NM 88002-5502
1	AFWL/SUL Kirtland AFB, NM 87117
1	Air Force Armament Laboratory ATTN: AFATL/DLODL (Tech Info Center) Eglin AFB, FL 32542-5000
10	C.I.A. OIR/DB/Standard GE47 HQ Washington, D.C. 20505
1	Commander US Army Aviation Systems Command ATTN: AMSAV-ES 4300 Goodfellow Blvd St. Louis, MO 63120-1798
1	AFELM, The Rand Corporation ATTN: Library-D 1700 Main Street Santa Monica, CA 90406
4	Ford Aerospace & Communications Corporation Ford Road ATTN: Charles O. White Bud Blair Ken Zeroll Chuck Rippe Newport Beach, CA 92660
3	Honeywell, Inc. 600 Second Street, NE ATTN: W.E. Martwick Ken Sundeen George Stilley Hopkins, MN 55343
5	Aerojet Ordnance Company Tustin Facility ATTN: Jim Parkinson Doug LaFevre Saul Wasserman Abe Flatou S.H. Rush 2521 Michelle Drive Tustin, California 92680
	Aberdeen Proving Ground
	Dir, USAMSAA ATTN: AMXSY-D AMXSY-MP, H. Cohen
	Cdr, USATECOM ATTN: AMSTE-SI-F
	Cdr, CRDEC, AMCCOM ATTN: SMCCR-RSP-A SMCCR-MU SMCCR-SPS-IL

U ER EVALUATION SHEET/CHANGE OF ADDRESS

This Laboratory undertakes a continuing effort to improve the quality of the reports it publishes. Your comments/answers to the items/questions below will aid us in our efforts.

1. BRL Report Number_____ Date of Report_____

2. Date Report Received_____

3. Does this report satisfy a need? (Comment on purpose, related project, or other area of interest for which the report will be used.)_____

_____

_____

4. How specifically, is the report being used? (Information source, design data, procedure, source of ideas, etc.)_____

_____

_____

5. Has the information in this report led to any quantitative savings as far as man-hours or dollars saved, operating costs avoided or efficiencies achieved, etc? If so, please elaborate._____

_____

_____

6. General Comments. What do you think should be changed to improve future reports? (Indicate changes to organization, technical content, format, etc.)

_____

_____

_____

CURRENT ADDRESS

_____
Name

_____
Organization

_____
Address

_____
City, State, Zip

7. If indicating a Change of Address or Address Correction, please provide the New or Correct Address in Block 6 above and the Old or Incorrect address below.

OLD ADDRESS

_____
Name

_____
Organization

_____
Address

_____
City, State, Zip

(Remove this sheet, fold as indicated, staple or tape closed, and mail.)